Beachrock: A tool for reconstructing relative sea level in the far-field

Barbara Mauz[1], Matteo Vacchi[2], Andrew Green[3], Goesta Hoffmann[4] and Andrew Cooper[5]

[1]School of Environmental Sciences, University of Liverpool, Liverpool L69 7ZT, UK
[2]Aix-Marseille Université, CEREGE CNRS-IRD UMR 34, Aix en Provence, France
[3]School of Agriculture, Earth and Environmental Sciences, University of KwaZulu-Natal, Private Bag X54001, Durban, South Africa
[4]German University of Technology in Oman, P.O. Box 1816, Athaibah, PC 130, Sultanate of Oman
[5]School of Environmental Sciences, University of Ulster, Coleraine BT52 1SA, UK

Abstract

Today's understanding of sea-level change developed through a combination of process-based physical modelling and observational data. These data were recorded from coral reefs in the far-field of the former ice sheets where a geographically variable relative sea-level signal is expected as a response of the earth to ocean loading. Given this variability and the limited geographical distribution of coral reefs, there is a need to explore other, non-coral based sea-level markers to further understand and 'fingerprint' melt-water. Here, we present beachrock, a coastal deposit suitable for relative sea-level (RSL) observations in the far-field. Beachrock is an intertidal deposit forming in the zone where carbonate saturated meteoric and marine water mix and pCO_2 decreases. We provide the conceptual framework for beachrock analysis and describe techniques suitable for analysing and dating the deposit. The approach is standardised by outlining the sediment characteristics in terms of RSL indicative meaning and indicative range, and is tested against published data. A study conducted on coasts of the Mediterranean Sea exemplifies the utility of beachrock for RSL reconstruction. It is shown that the precision of the reconstruction is derived from the combined uncertainty of burial age and tidal amplitude or tidal range. The uncertainty can be reduced to half the tidal amplitude when a deposit can be ascribed to the upper (or lower) intertidal zone. Beachrock-based data benefit from the lack of non-quantifiable error terms such as post sedimentary compaction due to the instantaneous formation and high preservation potential of the

deposit. This underlines the high precision of the RSL reconstruction using beachrock, a prime requirement for testing coral-based records.

1. Introduction

Observational data from many coasts around the world indicate that sea level is rising with as yet undetermined consequences for low-lying coasts (e.g., Nicolls and Cazenave, 2010). Extrapolation into the future suggests moderate sea-level rise, however, with a high degree of uncertainty, in particular at the regional scale. Informed decisions at a regional scale are highly dependent on precise sea-level projections, which improve the longer the regional relative sea-level (RSL) curve stretches back into the past. During the last deglaciation the sea level rose with both fast and slow velocities; a regional RSL curve that covers the last deglaciation therefore improves our understanding of the regional coastal response to various forms of sea-level rise.

In the far-field of the former ice sheets the relative sea-level signal varies due to the variable response of the earth to ocean loading. While the physics of this spatial variation is well understood, the effect of the mechanisms on a regional scale is poorly constrained due to insufficient observations over wider areas. While coral reef deposits are excellent RSL markers, the vertical living range of the coral species is large and their growth rate is not linear (Montaggioni, 2005). There is therefore a need to find alternative RSL markers that can be used to test the coral-based records from Tahiti and Barbados and to establish records where no coral markers are available (e.g., Livsey and Simms, 2013).

One of these markers is beachrock, a littoral deposit occurring predominantly in the far-field that is lithified almost instantaneously and thereby records the position of the corresponding shoreline. Many workers have studied the deposit and Vousdoukas et al. (2007) provided a comprehensive overview on formation, occurrence and relevant literature. After the early description of Stoddart and Cann (1965), the properties suitable for RSL reconstruction were first highlighted by Hopley (1986), but, in comparison to other RSL markers, beachrock remained understudied. Here, we highlight the properties of beachrock that are useful for RSL reconstruction and quantify associated uncertainties. We aim at providing the basic methodology for increasing the number of observational data in mid-latitudinal and far-field regions and at standardising the scientific approach of using beachrock as a RSL indicator. Using an example, we show how the beachrock can be transformed into a sea-level index point (SLIP) with well-defined indicative meaning and tidal datum. We discuss potential and limitation of the approach in the light of our own results and other published data.

2 Beachrock: Sea-level related characteristics

Beachrock is a lithified coastal deposit where lithification is a function of CO_3^{-2} ion concentration in seawater, microbial activity and degassing of CO_2 from seaward flowing groundwater. Field experiments (e.g., Hanor, 1978) and coastal observations (e.g., Hopley, 1986) suggest that cementation occurs within a few decades where suitable coastal morphology provides sufficient accommodation space for soft sediment to settle. Beachrock occurs as a single, isolated deposit with limited lateral continuity due to its dependence on suitable chemical conditions.

2.1 The sediment

Sediment that is suitable for transformation into rock on a decadal time scale needs to provide sufficient pore space for carbonate crystals to precipitate and grow. Typically, its texture is coarse silt to sand, sometimes with pebbles. The rate of sediment supply is limited in order for the diffusive transport of CO_2 through overlying sediment to be effective (Hanor, 1978) and for the carbonate factory to operate without perturbation. The cementation rate must therefore outpace the sedimentation rate for the rock to form.

Beachrock has sedimentary textures and bedding structures indicative of the upper shoreface to beach sedimentary environment where shoaling waves and longshore currents operate. The upper shoreface to foreshore environment is typically characterised by small asymmetrical ripple foreset laminae (Fig. 1), low angle laminar or foreset beds dipping seaward (Fig. 2) or by horizontal plane-parallel laminar beds, depending on the dip of the shore profile and flow criticality (see also Bezzerra et al., 1998). Between the wave-breaker surf zone and swash and back-wash zone a lag deposit may form. Towards land symmetrical ripples and horizontal bedding characterise the foreshore zone (Fig. 3). These structures vary depending on the morphology of the coast and its tidal and wave regime (e.g., Vieira et al. 2007).

The thickness and lateral extent of a beachrock deposit depends on both sediment supply and accommodation space. Thin (<2 m) and probably isolated beds form in pockets on reflective, bedrock-controlled coasts; these beds are larger on intermediate and dissipative coasts. Beachrocks may preserve antecedent morphologies such as coastline-parallel ridge and runnel-type features.

2.2 The cement

The cement by which the loose sand is locked into position is indicative of the nearshore zone between shoreface and beach, at the interface between seawater and meteroric water (Fig. 4). The interface is the mixing zone, the chemically most active zone, where beachrock forms. The zone is characterised by a pore fluid that is a mixture of different end-member solutions, originating from the adjacent environments (e.g. hypersaline waters from sabkhas; meteoric water from groundwater). The chemical characteristics of the solutions, in particular acidity and under- or supersaturation with respect to calcite, control the precipitation of the carbonate mineral when the initial pCO_2 falls due to degassing (Plummer, 1975). As a carbonate mineral will only precipitate from a solution that is supersaturated with respect to this mineral, the mixing of the groundwater and seawater must result in supersaturation. Plummer (1975) showed that for this to happen the mixture must contain more than 50% seawater, the end-member solutions are in equilibrium with calcite and the pCO_2 drops below 10^{-2} Atm (Fig. 5). The higher the temperature, the less seawater is required to achieve supersaturation (Fig. 6) and the more CO_2 escapes, the higher the pH and the faster carbonate minerals can precipitate. Thus, the sediment layer that is closest to the water table will cement first and fastest. If the end-member solution contains Mg^{2+}, high magnesian calcite (HMC) precipitates and the typical crystal form of this mineral is bladed or granular (Fig. 7B). The higher the temperature of the solution, the faster aragonite precipitates relative to calcite (Burton and Walter, 1987) and the crystal form the cement takes is mostly fibrous (Fig. 7C). Crystal arrangement and fabric is controlled by environment and gravitation. HMC and aragonite form circumgranular rim in meniscus fabric in the vadose environment (Fig. 7D) or symmetrical crusts in the meteoric environment. In most beachrocks the pore space is not completely occluded but is filled with mosaic fabric and may remain empty in the centre. Fig. 4 depicts the spatial relationship between carbonate cementation zones and Table 1 provides the details of the cement types in terms of crystal form, size and fabric.

Diagenesis takes place in the subsurface in response to a change in water-table elevation, temperature or pressure. Diagenesis involves processes such as dissolution, reprecipitation and recrystallisation and the end-point of these processes is chemical stability. The process follows the relative thermodynamic stability of magnesian calcite and aragonite and the chemistry of the pore fluid. The thermodynamic calculations reveal the metastability of aragonite with respect to calcite, and of magnesian calcite with respect to calcite and dolomite (Morse and Mackenzie, 1990). Most effective in terms of creating the end-members calcite and dolomite is the infiltration of meteoric water depleting the cement in Mg, Sr and Na and enriching it with other elements (e.g. Fe^{2+}).

Dissolution and subsequent creation of secondary porosity can occur through infiltration of meteoric water where the dissolution capacity of the water is largely controlled by the amount of dissolved CO_2 and the permeability of the arenite frame resulting often in molds and vugs. These can be later filled with marine cement or intraclasts.

The pathway of the diagenetic process is influenced by the original composition of the sediment. For example, coralline algae colonising the foreshore of many coasts, has the highest $MgCO_2$ content of all coastal magnesian calcite components (7-20 mol% MgCO3; Milliman, 1971) and is the least susceptible to replacement by calcite (Walter and Hanor 1979). In the Mediterranean calcite cement in algae has about 15 mol % MgCO3 and this cement is petrographically identical to beachrock cement in many regions (Alexandersson, 1985). HMC is thus the likely cement where red algae constitute part of the coastal sediment.

The diagenetic process can be reversed under the presence of foreign substances (e.g. orthophosphate from an overlying soil; Walter and Hanor, 1979) which changes the relative stability of the three carbonate minerals and thereby impacts on the preferential dissolution of one or the other carbonate mineral. The process can also be delayed, in particular in the presence of Mg, because geochemically, it functions as an inhibitor of carbonate precipitation. The less Mg the pore fluid contains, the larger calcite crystals and the less fragile the rock.

The burial history is thus characterised by cement phases and these phases can constitute compositional zoning (Meyers, 1974) on surfaces of components and in pore spaces. It is important to identify this zoning, mostly represented by carbonate fringes and granular mosaics, because diagenesis can obscure the beachrock origin and thus overprint its usefulness as a RSL indicator.

2.3 Preservation

The degree of preservation depends on the rate of sea-level change and the rate of lithification where the latter must exceed the rate of RSL change. The lithification is fastest from beach groundwater where larger crystals bind components. With increasing sea-water mixing the process is slower (Hanor, 1978); smaller carbonate crystals alongside high porosity make the rock more friable on the seaward side of the deposit. Under constant hydrodynamic conditions the landward part of a beachrock bed is therefore better preserved while its seaward part may be reworked under changing wave energy. We consider two types of reworking: synsedimentary and postsedimentary. As cementation is so rapid, contemporaneous reworking (e.g. by storm surge) is easily identified through intraclasts which become part of the deposit immediately after the high-magnitude event. If such an event occurs after deposition, parts of the deposit are displaced and deposited as boulders downdip or updip of the storm surge trajectory.

3 Suitable analytical techniques

Several standard techniques apply to beachrock analysis. These include: surveying to estimate elevation, mapping and logging to identify macroscopically lateral facies relationships and thin section-based petrographic microscopy to identify the depositional environment including the type of cement. Here, we highlight other suitable sediment analysis techniques less used in beachrock analysis and outline the two most suitable dating techniques.

3.1 Ground Penetrating Radar

Ground Penetrating Radar (GPR) is a fast, non-destructive and non-invasive geophysical method used for high-resolution mapping of the shallow subsurface. The method relies on short pulses of high frequency electromagnetic energy transmitted into the ground by a transmitting antenna. There, the waves are reflected in zones of contrasting material properties. The reflected waves are received by the system and the two-way travel time is recorded. The penetration depth of the radar-waves depends on the sediment, the water content and the antenna frequency. Depending on the frequency, the vertical resolution is in the range of a few centimeters and the penetration depth may be tens of meters. A 2D-cross section (radargram) is generated while moving the system along a line. The radargram reveals layer boundaries and sedimentary structures essential for correlation between outcrops and mapping of the stratigraphic architecture. Limitations of the method are high electrical conductivity in the subsurface (e.g. due to sea water intrusion) and fine-grained sediments (silt, clay) that reduce the penetration depths. GPR surveys on sandstones and other hardrock are a common procedure, whereas GPR surveys on beachrock (Fig. 8) have rarely been performed. Davis and Annan (1989), Bristow and Jol (2003) and Neal (2004) provide a general overview of this and Koster et al. (2014) describe the use of GPR in an arid coastal setting. As beachrocks are relatively thin deposits, high frequency antennas (400 MHz or higher) are appropriate for the scale of resolution required. Uplifted coastal areas where the beachrock is situated above the water table are prime targets for such GPR surveys.

3.2. Underwater mapping and sampling

A yet to explore number of beachrock deposits occur below modern mean sea level. Direct SCUBA diving techniques are suitable to describe and to sample beachrocks down to around 35 m water depth (Desruelles et al., 2009; Vacchi et al., 2012a). The exact water depth is recorded by averaging 2 electronic depth gauges with a precision of 0.5 m (at depths ≥ − 3 m). In shallower water, precise measures can be obtained using a 3 m metal bar with a precision ≤ 0.5 m (Rovere et al., 2010, 2011; Vacchi et al., 2012a, b).

3.3 Cathodoluminescence

This technique is a tool to identify type and zonation of the cement. The luminescence is a function of the relative concentration of Mn^{2+} as the primary activator ion and Fe^{2+} as the deactivator ion. Its intensity is controlled by the absolute amount of Mn^{2+} concentration, by the Fe/Mn ratio in calcite (Hemming et al., 1989) and by rate of crystal growth (Ten Have and Heijnen, 1985). The colours are visually categorised as bright, moderate, dull and non-luminescent. The early precipitation of carbonate cement is from oxidising pore water and this water is free of Mn and Fe so that the first zone is non luminescent. When the water begins to stagnate, Mn-bearing carbonate minerals precipitate and these emit yellow to red colours. The intensity of these colours is a function of the reducing conditions of the pore water and the extent to which Fe is exported. Thus, marine cement is virtually non-luminescent due to the positive Eh of sea water and changes to yellow-orange colours when the cement precipitates from more Eh-negative waters (Fig. 9). The spatial mix of colours may indicate repeated dissolution and precipitation phases cutting across crystal tops and isolation zones of earlier versus later cementation. Amieux et al. (1989) studied tropical beachrock and found primary cement of isopachous fibrous aragonite rim emitting very dull orange and blue colour; the pores were filled by equant crystals emitting a bright yellow-orange colour and larger equant crystals emitting dull blue and medium orange colours. The zonation was interpreted as indicating a progression from a marine to a freshwater environment, characterised by early marine cementation and subsequent early diagenesis in mixed water followed by freshwater.

3.4 Dating

Radiocarbon and optically stimulated luminescence (OSL) are the two most suitable dating techniques for determining a burial age of the deposit. OSL relies on the exposure of quartz grains to daylight. After burial, i.e. during formation of the beachrock, the grains are sheltered from daylight and acquire a luminescence signal by exposure to environmental radioactivity. For radiocarbon dating, shells or cement can be used. The accuracy of both techniques depends on the suitability of the material used for dating and a number of other requirements specific to the technique. For the OSL technique it is, amongst others, the ability to reconstruct the change of dose rate during burial (Nathan and Mauz, 2008). For radiocarbon it is the ability to correct for isotope fractionation and reservoir effects, in particular when cement is used because its carbon isotopes originate from two solutions with two different isotopic compositions. As a result both the marine reservoir effect and the terrestrial hardwater effect must be considered, which might be difficult in practice without information from additional stable isotopes (e.g., strontium).

Thomas (2009) was the first to employ the OSL technique to accurately date beachrock deposits occurring on the coast of southeast India. An OSL data set is listed in Tables 2. The sample from Torre Vieja demonstrates the importance of dating: its morphological setting (Fig. 10) suggests a deposit of Holocene age while its OSL age is around 80 ka suggesting that the RSL was situated at the modern level during MIS 5a.

A comparison between ages obtained from radiocarbon and OSL dating techniques shows systematically lower OSL ages regardless of the calibration curve used for radiocarbon, the differences within ^{14}C or whether whole rock or shell was used (Bosman, 2012). Ages obtained from mollusc shells tend to agree better with quartz OSL ages (Bosman, 2012). As such, careful selection of the material used for radiocarbon dating can circumvent the effect of old carbon (e.g., Desruelles et al. 2009).

4 Establishing a sea-level index point

To qualify as a sea-level index point (SLIP), the sea-level indicator has to be characterised by (1) location, (2) age, (3) sampling elevation and (4) indicative meaning which is the known relationship between the indicator and the corresponding shoreline (van de Plassche, 1986; Shennan, 1986). This known relationship is described by the reference water level and the midpoint of the indicative range where the indicative range is the elevation range occupied by the sea-level indicator

(Shennan, 1986; van de Plasche, 1986). The sea-level indicator with its known indicative range is converted into a SLIP once its age is known.

An undisturbed *in situ* beachrock is a sea-level indicator on the basis of its cement and its sediment texture and bedding structures. The clarity of its indicative meaning depends largely on the preservation of the original cement and the ability to link cement with other sedimentary information.

In the intertidal zone the metastable aragonite and HMC form as rim cements. This fabric linked with small-scale trough cross bedding is indicative of the lower intertidal zone. Its indicative range spans from mean low water level (MLW) to mean tidal level (MTL) and, using the midpoint of this zone as reference water level, the associated error is half the tidal amplitude ($a_1/2$, where a=tidal amplitude). When this fabric is linked with low angle seaward-dipping tabular cross bedding and keystone vugs, the indicative range spans from MTL to mean high water level (MHW) and the error term is $a_2/2$. In the absence of sediment bedding information, the indicative range associated with the intertidal cement fabrics ranges from the MLW to the MHW. The zone is called 'undifferentiated intertidal' and its error term is a_1+a_2 which is the average tidal range.

Samples exhibiting sparitic cements infilling cavities, micrite forming meniscus between grains and internal sediments as geopedal infilling are characteristic of the vadose zone. The relationship of these samples with a former tidal level is the upper intertidal zone and the spray zone. The elevation of this zone depends on wave exposure and the local geomorphology (Leeuw et al., 2000). For error calculation we include the spray zone due to its potential contribution to the cementation so that the error term is $(a_2/2)+s$, where s is the elevation of the spray zone. Low angle seaward-dipping tabular cross bedding with keystone vugs provide an upper intertidal indicative range (but no example for this assemblage was found in literature). In the absence of sediment bedding information, samples exhibiting these types of cement fabric provide a terrestrial limiting point (i.e. MTL is situated below this point). Likewise, samples showing LMC equant spar crystals (typically consisting of equigranular, anhedral to subhedral crystals) formed near or above the high tide and represent a terrestrial limiting point.

Where only sediment bedding information is available, the indicative meaning is less precise. Small-scale trough cross-bedding is generally evidence of the lower intertidal environment (Strasser and Davaud, 1986; Bezerra et al., 2003; Caldas et al., 2006) and without cement information, such samples represent a marine limiting point (i.e. MTL is above this point). Likewise, low angle seaward dipping tabular cross bedding indicates upper intertidal to supratidal formation (Bezerra et al., 2003) and without cement information, these samples should be used as a terrestrial limiting point (i.e. MTL is below this point). However, in the presence of keystone vugs, an indicative range from MTL to MHW with an error term of $a_2/2$ can be ascribed (Dunham, 1970; Strasser and Davaud, 1986). Notwithstanding this evidence, marine cements should be present to ascribe the sample to the upper intertidal zone (Desruelles et al., 2009). A summary of indicative meaning and error terms is provided in Table 3 and Fig. 11.

The total uncertainty of this vertical shoreline reconstruction is quantified from levelling, indicative range (as described above) and tidal range, applying the square root rule. We assume negligible beachrock formation in the zone of the highest tide and use the spring/neap tide range as an error of tidal range. Other potential errors such as changes in the water table and sediment compaction are regarded as negligible due to the instantaneous cementation of the sediment.

5 Relative sea-level reconstruction using beachrock

We outline previous work where beachrock was used for RSL reconstruction. The most comprehensive studies are described in the text and other relevant studies are listed in Table 3. The compilation focuses on sediment characteristics and techniques used to determine a SLIP and builds on the review of Vousdoukas et al. (2007) where formation and cementation processes as well as criteria for identification are described. The map in Fig. 12 displays the spatial distribution of beachrock-based RSL reconstructions listed in Table 4.

Most authors used the cement type to infer the position of the shoreline with uncertainties between 0.5 m and 1.5 m (Table 3). The standard setting for this approach was Strasser et al. (1989) who used data from field surveying, petrography, microprobe and SEM analyses to infer timing of cementation and migration of shoreline.

Desruelles et al. (2009) built on the example of Strasser et al (1989) and determined the indicative meaning through SEM, petrographic and cathodoluminescence analyses and used keystone vugs to determine the position of the sea level with a precision of ±0.25-0.50 cm. The radiocarbon age of the deposits was obtained using the cement and the ages seem to confirm that the hand-picked samples were not contaminated by external carbonate. Studying details of the cement, Vacchi et al. (2012a) found primary marine phreatic cement, typical for the intertidal zone, followed by meteoric cement and bioclast dissolution. These findings allowed the authors to correlate the beachrock with other RSL indicators in order to reconstruct palaeo-shorelines in distinct tectonic domains.

Some authors combined evidence from cement, sediment bedding and local features to reconstruct the shoreline. Michelli (2008) and Stategger et al. (2013) linked saltmarsh, mangrove and beachrock deposits to reconstruct the RSL. The relationship of each sample with the contemporary tidal levels was assessed through sediment bedding and cement analysis. Radiocarbon dating was performed on well preserved marine shells and coral fragments in beachrock samples. Ramsay (1995) established a RSL curve based entirely on beachrock observational data. The indicative meaning was deduced from the present-day beach where beachrock forms at 10-20 cm above mean sea level and from the presence of aragonitic rim cements. These were interpreted as indicating shoreline position with an uncertainty of 0.5 m (Ramsay 1995). The modern beachrock deposits were later ascribed to the intertidal environment due to their position at mean low tide level and the cementation by micritic, aragonitic and iron oxide infilled voids (Cawthra and Uken, 2012). Cawthra et al. (2012) revisited these deposits and found micritic coatings followed by isopachous prismatic crystal rims and equant calcite spars in pores often capped by cryptocrystalline coatings. On the basis of this two-step cementation history, alongside trough cross-bedded and often heavy mineral lined foresets, the depositional environment was considered intertidal, analogous with the low tide trough of contemporary beaches. Bosman (2012) confirmed the intertidal environment and determined a 2 m uncertainty based on the position of the modern beachrock and the tidal range.

Bezerra et al. (1998) attributed medium to coarse sandstone that was deposited in seaward dipping cross-stratified beds with increasing grain size seawards, to the middle to lower foreshore with a RSL precision of ±1 m. With medium to fine sandstone the upper shoreface part of the deposit was identified and the corresponding position of the shoreline was estimated with an error of ±0.5 m. Vieira et al. (2007) refined this approach by mapping out lithofacies with distinct characteristics relevant for the position of the corresponding shoreline.

A few authors have used the associated coastal fauna. Yaltirak et al. (2002) identified the beachrock deposits situated in various altitudes above modern sea level through the presence of the fauna *Balanus*, *Alvania lacteal* and *Truncatella subcylindrica* and deduced the indicative meaning through comparison with the modern analogue. In this study U-series dating on shells was employed resulting in consistent MIS 5e and MIS 7 ages but also with some age reversals and unexplained age differences.

Beachrock deposits occur not only on modern coasts above or a few meters below water level, but also on submerged continental shelves where access is more challenging. Bosman (2012) used high-resolution geophysical profiling and sampling to establish a geological map that included 3 distinct beachrock ridges situated in around 25 m water depth. Using a similar method, Locker et al. (1996) mapped 4 distinct ridges partly composed of beachrock, which occur between 120 m and 60 m water depth. Two of these ridges may have recorded the meltwater pulse 1A. This and subsequent studies (Jarrett et al., 2005; Gardner et al., 2007) show also, that laterally continuous shoreline deposits can form at the edge of the inner shelf in places where the steepness of the slope is reduced to around 0.02 m/m.

6 Example

We highlight an example where beachrock data collected from an outcrop was used to infer the local RSL history.

In the Gulf of Gabès (south Tunisia) RSL observational data were generated through conventional field mapping, logging and elevation measurements using differential GPS. Present-day mean low and high tide shorelines were mapped from morphological evidence. Mean tidal range and mean astronomical tidal range were obtained from tide gauge data (station Ganouch; Sammari et al. 2006) and were taken into account to estimate the indicative range and its error. Texture, composition and matrix properties of sediment samples were identified from thin sections, and the carbonate mineralogy was studied using cathodoluminescence. OSL dating of quartz and radiocarbon dating of mollusc shells (Morhange and Pirazzoli, 2005) were used for age estimation.

In the coastal cross-section (Fig. 13) the succession of two beachrock deposits was identified. One is composed of planar beds of moderately sorted oolitic grainstone with isopachous HMC rim and scalenohedral dog tooth cement (Fig. 9A). Its age is around 6 ka and its elevation is 1.1±0.22 m. Onlapping this is a well-sorted mixed bio-siliciclastic grainstone with circumgranular HMC, which is blue in CL with an outer band of violet colour (Fig. 10B). Its age is around 4 ka and its elevation is 0.0±0.23 m.

Oolitic grainstone with isopachous HMC rim formed in the lower intertidal and was subsequently subjected to the upper intertidal. Assuming the geometry of this tectonically stable coast has not changed during the Holocene and the mean tidal range was therefore constant at 0.85±0.2 m, the indicative meaning of both SLIPs is -0.4±0.2 m. With the reference water level being the midpoint of the intertidal deposit, the shoreline of the mid Holocene deposit was then reconstructed to 1.4±0.4 m and the one of the onlapping deposit to 0.2±0.4 m. The error is derived from $\sqrt{a^2 + b^2 + c^2}$, where a, b, c are the independent error terms of levelling, tidal range and indicative meaning respectively.

7. Discussion

Beachrock forms in the mixing zone between the upper shoreface and the beach where sand-sized sediment is available and the morphology is suitably flat. The criteria to identify the sub-environment are based on cement and bedding structure where the cement should be described in terms of chemistry, crystal form and fabric. Integration of these criteria allows establishing indicative meaning and vertical error and resolves doubts (cf., Kelletat, 2006).

Occurrence, shelf morphology and RSL change

Beachrock deposits are unlikely to occur on the outer shelf where a steep gradient creates reflective beach morphologies. The use of beachrock for sea-level reconstruction is therefore restricted to the interval between post-glacial and pre-glacial when the sea level is situated on the shelf, and, in many cases, on the inner shelf. It is unlikely that beachrock forms a large-scale feature on the shelf when RSL rise exceeds ~12 mm/a because the shoreface (main source of sediment for the intertidal zone on subtropical coasts) is reworked at a rate that precludes preservation. Beachrock can form in patches when RSL rise is <12 mm/a because sufficient sediment would be available in places and, after 20 years of lithification time, the RSL would still be within the intertidal zone. Beachrock forms on a larger spatial scale with RSL rise < 5mm/a (Voudoukas et al., 2007). As Quaternary RSL falls on average with a slower rate than it rises, it can be hypothesised that most of the beachrock fields represent a falling RSL. Either way, beachrock formation does not require a RSL stillstand; more important is a continuous and almost constant carbonate accumulation rate when sea-surface temperature (SST) falls during cool climate periods. For example, in the oligotrophic western (sub-)tropical Atlantic where beachrock fields are frequent, carbonate accumulation was nearly constant during the last glacial/interglacial transition (Arz et al., 1998) so that the carbonate factory did not slow down during cool climate periods. But this might not have been the same elsewhere and continuous beachrock formation in cooling coastal waters remains to be shown by data from the currently inundated shelves.

Cement

There was a considerable amount of confusion about the interplay between cementation processes and geomorphological position leading some authors to express misgivings on the reliability of beachrock as a sea-level indicator (e.g., Kelletat, 2006) with subsequent discussion (Knight 2007). The comprehensive review of Vousdoukas (2007) has removed these doubts and clarified that the cement is crucial for identifying the spatial relationship between coastline and beachrock formation zone. This key element in RSL reconstruction can be masked by multiple phases of rim cement formation, dissolution or other geochemical reorganisation where the pathway of diagenesis is dependent on the original mineralogy of the sediment undergoing alteration and on the chemistry of the overlying bed. While staining and cathodoluminescence are excellent tools to establish cement zoning, this analysis is probably the most challenging part of the SLIP investigation. The typical reorganisation with rising RSL is micritisation of biotic and abiotic calcite and aragonite, dolomitisation in the sulphate reduction zone and with falling sea level it is dissolution and recrystallisation of aragonite to calcite and HMC to LMC. In case of complete diagenesis the depositional origin may be hard to identify.

The cementation rate is most rapid in the landward side of the beachrock formation zone where large carbonate crystals fill pore space and bind components within the space of years to decades. Thus, before burial the sediment is already lithified and is likely not subject to compaction that would be significant enough to impact on the vertical precision of the SLIP.

<u>Chronology</u>

Suitable techniques to determine the age of a beachrock sample are OSL and radiocarbon. U-series, in particular when using mollusc shells is unsuitable (Kaufman et al., 1971; Mauz and Antonioli, 2009) due to the significant geochemical alterations and associated uranium isotope ratio and profile across the shell. There are many examples that show that even corals, in particular non-tropical species, suffer from diagenetic alteration impacting on the accuracy of an age derived from U-series technique (e.g., Leeder et. al., 2003; Amorosi et al., 2014).

<u>Precision</u>

Hopley (1986) expressed concerns with regard to height relationships because the upper limit of cementation would not be well defined. Indeed, given the potential impact of sea-water spray on the cementation, the limits of the former intertidal zone cannot be determined on the basis of the cement alone; information on the tidal regime is also required. Ideally, lateral facies relationships based on a transect across and beyond the beachrock formation zone is also established.

Beachrock is an intertidal deposit. The vertical error of the RSL reconstruction is therefore a result of the 3 error terms derived from levelling, indicative range and tidal range. The precision can be raised up to half of the tidal amplitude by combining cement with facies analysis. Most beachrocks occur on microtidal coasts with an average thickness of 2 m (e.g., Cooper, 1991); thus, the vertical errors typically fall between 2 m and 0.1 m. While these error bars are comparable to RSL reconstructions derived from saltmarshes (e.g., Barlow et al., 2013), they are bigger than those derived from microbial mats (Livsey and Simms, 2013). They benefit, however, from the lack of additional error terms that are hard to quantify (e.g., compaction). The beachrock-based reconstruction can be an order of magnitude more precise than that obtained from corals. Notwithstanding this, any direction of shoreline migration is hard to infer from beachrock. The deposit is usually a singularity and lacks backstepping or prograding architecture and related bounding surfaces.

8. Conclusions

We have shown that a beachrock deposit is a reliable RSL marker. It can be used to increase the number of RSL observations in the far-field and it can be used to test coral-based RSL records. The error of the beachrock-based RSL reconstruction is comparable to other RSL markers with the advantage that there are no additional, hard to quantify error terms.

A beachrock deposit is not continuous, but a point in time and space. Its zone of formation is limited to coasts with low sedimentation rate, relatively flat morphology and warm SST. How a drop in SST impacts on the continuity of formation at any particular location remains to be shown by investigating currently inundated shelves in the far-field.

Acknowledgements

We wish to acknowledge N Porat, E Galili, D Sivan, S Regan, N Elmjdoub, E Abdulsamad, M Egwiten, S Emhanna, A Aljazwi and K Areig, - all helping in the field with collecting samples at variously remote coastlines. We are grateful to S Packman for the hard work with the hard samples in the OSL laboratory and Suzanne Yee for her help with the cartographic work. MV is grateful to the Labex OT-Med (n° ANR-11-LABX-0061) funded by the French government through the A*MIDEX project (n° ANR-11-IDEX-0001-02). GH acknowledges financial support by The Research Council Oman (TRC-grant ORG GUtech EBR 10 013) and BM is grateful to the Royal Geographical Society for supporting field work in the Oman.

References

Al-Ramadan, K. 2013. Diagenesis of Holocene beachrocks: A comparative study between the Arabian Gulf and the Gulf of Aqaba, Saudi Arabia. Arabian Journal of Geosciences; DOI 10.1007/s12517-013-1127-7.

Alexandersson, T., 1985. Carbonate cementation in recent Coralline algal constructions, in, Toomey, D.F. and Nitecki, M.H. (eds), *Paleoalgology: Contemporary Research and Applications*. Springer Verlag Berlin Heidelberg, p. 261-269.

Amieux, P., Bernier, P., Dalongeville, R. and Medwecki, V., 1989. Cathodoluminescence of carbonate-cemented Holocene beachrock from Togo coastline (West Africa): An approach to early diagenesis. Sedimentary Geology 65, 261-272.

Amorosi, A., Antonioli, F., Bertini, Marabini, S., Mastronuzzi, G., Montagna, P., Negri, A., Rossi, V., Scarpone, D., Taviani, M., Angeletti, L., Piva, A. and Vai, G.B., 2014. The Middle-Upper Pleistocene Fronte Section (Taranto, Italy): An exceptionally preserved marine record of the Last Interglacial. Global and Planetary Change 119, 23-38.

Arrieta, N., Goienaga, N., Martinez-Arkarazo, I., Murelaga, X., Baceta, J. I., Sarmiento, A. and Madariaga, J. M. (2011). Beachrock formation in temperate coastlines: Examples in sand-gravel beaches adjacent to the Nerbioi-Ibaizabal Estuary (Bilbao, Bay of Biscay, North of Spain). *Spectrochimica Acta Part A: Molecular and Biomolecular Spectroscopy*, *80*(1), 55-65.

Arz, H.W., Paetzold, J. and Wefer, G., 1998. Correlated Millennial-Scale Changes in Surface Hydrography and Terrigenous Sediment Yield Inferred from Last-Glacial Marine Deposits off Northeastern Brazil. Quaternary Research 50, 157-166.

Badve, R.M., Rajshekhar, C., Kumaran, K.P.N., Kamble, C.V., 1997. On the age and fauna of beachrock of Kegaon Coast, Uran, Maharashtra. Current Science 72 (3), 168.

Bakler, N., Neev, D. and Magaritz, M., 1985. Late Holocene tectonic movements at Tel Haraz, southern coast of Israel. Earth and Planetary Science Letters 75(2), 223-230.

Barlow, N., Shennan, I., Long, A.J., Gehrels, W.R., Saher, M.H., Woodroffe, S.A. and Hillier, C., 2013. Salt marshes as late Holocene tide gauges. Global and Planetary Change 106, 90-110.

Bezerra, F.H.R., Lima-Filho, F.P., Amaral, R.F., Caldas, L.H.O. and Costa-Neto, L.X., 1998. Holocene coastal tectonics in coastal Brazil, in, Steward, I.S. and Vita-Finzi, C. (eds), *Coastal tectonics*. Geological Society, London, Special Publications 146, 279-293.

Bezerra, F.H.R., Barreto, A.M.F. and Suguio, K., 2003. Holocene sea-level history on the Rio Grande do Norte State coast, Brazil. Marine Geology 196, 73-89.

Bosman, C., 2012. The marine geology of the Aliwal Shoal, Scottburgh, South Africa. PhD thesis, University of KwaZulu-Natal, Durban, 581 p.

Bristow, C.S. and Jol, H.M., 2003. An introduction to ground penetrating radar (GPR) in sediments. – Geological Society, London, Special Publications 211 (1), 1-7.

Burton, E.A. and Walter, L.M., 1987. Relative precipitation rates of aragonite and Mg calcite from seawater: Temperature or carbonate ion control? Geology 15, 111-114.

Caldas, L.H., Stattegger, K. and Vital, H., 2006. Holocene sea-level history: Evidence from coastal sediments of the northern Rio Grande do Norte coast, NE Brazil. Marine Geology 228, 39-53.

Calvet, F., Cabrera, M. C., Carracedo, J. C., Mangas, J., Pérez-Torrado, F. J., Recio, C., Travé, A., 2003. Beachrocks from the island of La Palma (Canary Islands, Spain). Marine Geology 197(1), 75-93.

Caron, V., 2012. Geomorphic and sedimentologic evidence of extreme wave events recorded by beachrocks: a case study from the Island of St. Bartholomew (Lesser Antilles). Journal of Coastal Research 28, 811-828.

Cawthra, H. and Uken, R., 2012. Modern beachrock in Durban, KwaZulu-Natal. Afr J Sci. 2012;108(7/8), Art. #935, 5 pages. http:// dx.doi.org/10.4102/sajs. v108i7/8.935.

Cawthra, H.C., Uken, R., Ovechkina, M.N., 2012. New insights into the geological evolution of the Durban Bluff and adjacent Blood Reef, South Africa. South African Journal of Geology 115.3, 291-308.

Cooper, J.A.G., 1991. Beachrock formation in low latitudes: implications for coastal evolutionary models. Marine Geology, 98: 145–154

Davis, L. J. and Annan, A. P. (1989): Ground-penetrating radar for high-resolution mapping of soil and rock stratigraphy. - Geophysical Prospecting, 37: 531-551.

Desruelles, S., Fouache, E., Ciner, A., Dalongeville, R., Pavlopoulos, K., Kosun, E., Coquinot, Y. and

Potdevin, J.-L., 2009. Beachrocks and sea level changes since Middle Holocene: Comparison between the insular group of Mykonos–Delos–Rhenia (Cyclades, Greece) and the southern coast of Turkey. Global and Planetary Change.

Dunham, R.J. 1970. Keystone vugs in carbonate beach deposits. Bulletin of the American Association of Petroleum Geologist 45, 845.

El Sayed, M.K.H., 1988. Beachrock cementation in Alexandria, Egypy. Marine Geology 80, 29-35.

Erginal, A.E., Ekinci, Y.L., Demirci, A., Bozcu, M., Ozturk, M.Z., Avioglu, M. and Oztura, E., 2013. First record of beachrock on Black Sea coast of Turkey: Implications for Late Holocene sea-level fluctuations. Sedimentary Geology 294, 294-302.

Erginal, A.E., 2012. Beachrock as evidence of sea-level lowstand during the classical period, Parion antique city, Marmara Sea, Turkey. Geodinamica Acta 25(1-2), 96-103.

Friedman, G.M., 2011. Beachrocks record Holocene events, including natural disasters. Carbonates and Evaporites 26, 97–109.

Fuzhi, B., and Youshen, Y., 1988. Study on the “beachrock field” in Haishan Island, Guangdong Province. Chinese Journal of Oceanology and Limnology, 6(4), 343-357.

Galbraith, R.F. and Roberts, R.G., 2012. Statistical aspects of equivalent dose and error calculation and display in OSL dating: An overview and some recommendations. Quaternary Geochronology 11, 1-27.

Gardner, J V., Calder, B.R., Hughes Clark, J.E., Mayer, L.A., Elston, G., Rzhanov, Y., 2007. Drowned shelf-edge deltas, barrier islands and related features along the outer continental shelf north of the head of De Soto Canyon, NE Gulf of Mexico. Geomorphology 89, 370-390.

Ghandour, I. M., Al-Washmi, H. A., Bantan, R. A., and Gadallah, M. M., 2014. Petrographical and petrophysical characteristics of asynchronous beachrocks along Al-Shoaiba Coast, Red Sea, Saudi Arabia. Arabian Journal of Geosciences 7, 355-365.

Gischler, E. and Lomando, A.J., 1997. Holocene cemented beach deposit in Belize. Sedimentary Geology 110, 277-297.

Hanor, J.S., 1978. Precipitation of beachrock cements: Mixing of marine and meteoric waters *vs*. CO_2-degassing. Journal of Sedimentary Petrology 48, 489-501.

Hemming, N.G., Meyers, W.J. and Grams, J.C., 1989. Cathodoluminescence in diagenetic calcites: the roles of Fe and Mn as deduced from electron probe and spectrophotometric measurements. Journal of Sedimentary Petrology 59, 404-411.

Hoffmann, G., Rupprechter, M. and Mayerhofer, C., 2013. Review of the long-term coastal evolution of Oman – subsidence versus uplift. Zeitschrift der deutschen Gesellschaft für Geowissenschaften 164, 237–252.

Holail, H. and Rashed, M., 1992. Stable isotopic composition of carbonate-cemented recent beachrock along the Mediterranean and the Red Sea coasts of Egypt. Marine Geology 106, 141-148.

Hopley, D., 1986. Beachrock as a sea-level indicator. In: Van de Plassche O. (ed), Sea-level Research: a manual for the collection and evaluation of data. Geo Books, Norwich, pp. 157–173.

Jarrett, B.D., Hine, A.C., Halley, R.B., Naar, D.F., Locker, S.D., Neumann, A.C., Twichell, D., Hu, C., Donahue, B.T., Jaap., W.C., Palandro, D., Ciembronowicz, K., 2005. Strange bedfellows—a deep-water hermatypic coral reef superimposed on a drowned barrier island; southern Pulley Ridge, SW Florida platform margin. Marine Geology, 214, 295–307.

Kaufman, A., Broecker, W.S., Ku, T.L. and Thurber, D.L., 1971. The status of U-series methods of mollusc dating. Geochimica et Cosmochimica Acta 35, 1115–1183.

Kelletat, D., 2006. Beachrock as sea-level indicator? Remarks from a geomorphological point of view. Journal of Coastal Research 22, 1555–1564.

Kindler, P. and Bain, R. J., 1993. Submerged Upper Holocene beachrock on San Salvador Island, Bahamas: implications for recent sea-level history. Geologische Rundschau, *82*(2), 241-247.

Knight, J., 2007. Beachrock reconsidered. Discussion of: Kelletat , D., 2006. Beachrock as sea-level indicator? Remarks from a geomorphological point of view. Journal of Coastal Research, 22(6), 1558–1564. Journal of Coastal Research 234, 1074–1078.

Koster, B., Hoffmann, G., Grützner, C. and Reicherter, K., 2014. Ground penetrating radar facies of inferred tsunami deposits on the shores of the Arabian Sea (Northern Indian Ocean). Marine Geology 351, 13-34.

Lambeck, K., Antonioli, F., Purcell, A. and Silenzi, S., 2004. Sea-level change along the Italian coast for the past 10,000 yr. Quaternary Science Reviews 1567-1598.

Leeuw, G., Neele, F. P., Hill, M., Smith, M. H., Vignati, E. 2000. Production of sea spray aerosol in the surf zone. Journal of Geophysical Research: Atmospheres (1984–2012), 105(D24), 29397-29409.

Livsey, D. and Simms, A.R., 2013. Holocene sea-level change derived from microbial mats. Geology 41, 971-974.

Leeder, M.R., McNeill, L.C., Collier, R.E.L1, Portman, C., Rowe, P.J., Andrews, J.E. and Gawthorpe, R.L., 2003. Corinth rift margin uplift: New evidence from Later Quaternary marine shorelines. Geophysical Research Letters 30, NO. 12, 1611, doi:10.1029/2003GL017382.

Locker, S.D., Hine, A.C., Tedesco, L.P. and Shinn, E.A., 1996. Magnitude and timing of episodic sea-level rise during the last deglaciation. Geology 24, 827-830.

Mauz, B. and Antonioli, F., 2009. Comment on “Sea Level and Climate Changes during OIS 5e in the Western Mediterranean” by T. Bardají, J.L. Goy, J.L., C. Zazo, C. Hillaire-Marcel, C.J. Dabrio, A. Cabero, B. Ghaleb, P.G. Silva, J. Lario, Geomorphology 104 (2009). Geomorphology 110, 227-230.

Meyers, W.J., 1974. Carbonate cement stratigraphy of the Lake Valley Formation (Mississippian) Sacromento Mountains, New Mexico. Journal of Sedimentary Petrology 44, 837-861.

Meyers, W.J., 1987. Marine vadose beachrock cementation by cryptocrystalline magnesian calcite – Maui, Hawaii. Journal of Sedimentary Petrology 57, 558-570.

Michelli, M. 2008. Sea-level changes, coastal evolution and paleoceanography of coastal waters in SE-Vietnam since the mid-Holocene. Ph.D. Thesis, Christian-Albrechts-Universität Kiel, Germany, 159 pp.

Milliman, J.D., Gastner, M, and Müller, J., 1971. Utilization of magnesium in coralline algae. Geol. Soc. Am. Bull. 82, 573-580.

Milne, G.A., Long, A.J. and Bassett, S.E., 2005. Modelling Holocene relative sea-level observations from the Caribbean and South America. Quaternary Science Reviews 24, 1183–1202.

Mohange, C. and Pirazzoli, P., 2005. Mid-Holocene emergence of southern Tunisian coasts. Marine Geology 220, 205-213.

Montaggioni, L.F., 2005. History of Indo-Pacific coral reef systems since the last glaciation: Development patterns and controlling factors. Earth Science Reviews 71, 1-75.

Moore, C.H., 1973. Intertidal carbonate cementation, Grand Cayman, West Indies. Journal of Sedimentary Petrology 43, 591-602.

Morse, J.W. and Mackenzie, F.T., 1990. Geochemistry of sedimentary carbonates. Developments in Sedimentology 48. Elsevier, 707p.

Nathan, R.P. and Mauz, B., 2008. On the dose-rate estimate of carbonate-rich sediments for trapped charge dating. Radiation Measurements 43, 14-25.

Neal, A., 2004. Ground-penetrating radar and its use in sedimentology: principles, problems and progress. Earth-Science Reviews 66, 261-330.

Neumeier, U., 1998. Experimental modelling of beachrock cementation under microbial influence. Sedimentary Geology 126, 35-46.

Nicolls, R.J. and Cazenave, A., 2010. Sea-level rise and its impact on coastal zones. Science 328, 1517-1520.

Plummer, L.N., 1975. Mixing of sea water with calcium carbonate ground water. Geol. Soc. Amer. Memoir 142, 219-236.

Ramsay, P.J. and Cooper, J.A.G., 2002. Late Quaternary Sea-Level Change in South Africa. Quaternary Research, 57, 82–90.

Ramsay, P.J., 1995. 9000 Years of sea-level change along the southern African coastline. Quaternary International 31, 71–75.

Rey, D., Rubio, B., Bernabeu, A. M., and Vilas, F. (2004). Formation, exposure, and evolution of a high-latitude beachrock in the intertidal zone of the Corrubedo complex (Ria de Arousa, Galicia, NW Spain). Sedimentary Geology, 169, 93-105.

Rovere, A., Vacchi, M., Firpo, M., Carobene, L., 2011. Underwater geomorphology of the rocky coastal tracts between Finale Ligure and Vado Ligure (western Liguria, NW Mediterranean Sea). Quaternary International 232(1), 187-200.

Rovere, A., Parravicini, V., Vacchi, M., Montefalcone, M., Morri, C., Bianchi, C. N., Firpo, M., 2010. Geo-environmental cartography of the marine protected area "Isola di Bergeggi"(Liguria, NW Mediterranean Sea). Journal of Maps, 6(1), 505-519.

Sammari, C., Koutitonsky, V.G., Moussa, M., 2006. Sea level variability and tidal resonance in the Gulf of Gabès, Tunisia. Continental Shelf Research 26, 338-350.

Shen, J. W., Long, J. P., Pedoja, K., Yang, H. Q., Xu, H. L., and Sun, J. L., 2013. Holocene coquina beachrock from Haishan Island, east coast of Guangdong Province, China. Quaternary International, 310, 199-212.

Shennan, I., 1986. Flandrian sea-level changes in the Fenland. II: Tendencies of sea-level movement, altitudinal changes, and local and regional factors. Journal of Quaternary Science 1, 155-179.

Siesser, W. G., 1974. Relict and recent beachrock from southern Africa. Geological Society of America Bulletin, 85, 1849-1854.

Spurgeon, D., Davis Jr, R. A., and Shinnu, E. A., 2003. Formation of 'Beach Rock' at Siesta Key, Florida and its influence on barrier island development. Marine Geology, 200, 19-29.

Stattegger, K., Tjallingii, R., Saito, Y., Michelli, M., Thanh, N.T. and Wetzel, A., 2013. Mid to late Holocene sea-level reconstruction of southeast Vietnam using beachrock and beach-ridge deposits. Global and Planetary Change 110, 214-222.

Stoddart, D.R. and Cann, J.R., 1965. Nature and origin of beach rock. Journal of Sedimentary Petrology 35, 243-247.

Strasser, A. and Davaud, E., 1986. Formation of Holocene limestone sequences by progradation, cementation, and erosion. Two examples from the Bahamas. Journal of Sedimentary Petrology 56, 422-428.

Strasser, A., Davaud, E. and Jedoui, Y., 1989. Carbonate cements in Holocene beachrock: example from Bahiret el Biban, southeastern Tunisia. Sedimentary Geology 62, 89-100.

Ten Have, T. and Heijen, W., 1985. Cathodoluminescene activation and zonation in carbonate rocks: an experimental approach. Geologie en Mijnbouw 64, 297-310.

Thomas, P.J., 2009. Luminescence Dating of beachrock in th southeast coast of India – Potential for Holocene shoreline reconstruction. Journal of Coastal Research 25, 1-7.

Vacchi, M., Rovere, A., Zouros, N., Desruelles, S., Caron, V. and Firpo, M., 2012a. Spatial distribution of sea-level markers on Lesvos Island (NE Aegean Sea): Evidence of differential relative sea-level changes and the neotectonic implications. Geomorphology 159-160, 50-62.

Vacchi, M., Rovere, A., Schiaffino, C. F., Ferrari, M., 2012b. Monitoring the effectiveness of re-establishing beaches artificially: methodological and practical insights into the use of video transects and SCUBA-operated coring devices. Underwater Technology-Journal of the Society for Underwater Technology 30(4), 201-206.

van de Plassche, O., 1986. Sea-level Research: A manual for the collection and evaluation of data. Geo Books, Norwich, pp. 157–173.

Vieira, M.M., De Ros, L.F. and Bezerra, F.H.R., 2007. Lithofaciology and palaeoenvironmental analysis of Holocene beachrocks in northeastern Brazil. Journal of Coastal Research 23, 1535-1548.

Vousdoukas, M.I., Velegrakis, A.F. and Plomaritis, T.A., 2007. Beachrock occurrence, characteristics, formation mechanisms and impacts. Earth-Science Reviews 85, 23-46.

Walter, L.M. and Hanor, J.S., 1979. Orthophosphate: Effect on the relative stability of aragonite and magnesian calcite during early diagenesis. Journal of Sedimentary Petrology 49, 937-944.

Yaltirak, C., Sakinç, M., Aksu, A. E., Hiscott, R. N., Galleb, B. and Ulgen, U. B. 2002. Late Pleistocene uplift history along the southwestern Marmara Sea determined from raised coastal deposits and global sea-level variations. Marine Geology 190, 283-305.

Figures

Fig. 1. Cross-bedded beachrock at the seaward end of beachrock deposit at 1 m water depth. Tidal range is around 0.2 m (Naxos Island, Mediterranean Sea, 37,09° N 25,36° E; (see hammer of 35 cm length for scale).

Fig. 2. Beachrock showing low angle trough cross bedded foreset beds dipping seaward (above dashed black line).

Fig. 3. Beachrock showing horizontal bedding (below dashed black line) and planar forest beds. Each sediment package is around 25 cm thick.

Fig. 4. Schematic illustration of the coast and its zones of cement fabrics, preferred carbonate geochemistry and sediment bedding structures. Beachrock form in the mixing zone which includes the marine-vadose and the marine-phreatic environment.

Fig. 5. Calcite saturation index for mixtures of solutions that were saturated with calcite at different pCO_2 at 25 °C and pH of 7.5 (Plummer 1975).

Fig. 6. Calcite saturation index for mixtures of solutions that were in equilibrium with calcite at $10^{-2.5}$ Atm and 25 °C (Plummer 1975).

Fig. 7. Various cement types forming in the intertidal mixing zone. A - Isopachous rim cement composed of microcrystalline HMC; B – small calcite crystals filling pore space in granular fabric; C – Fibrous aragonite crystals growing normal on surface of quartz grains.

Fig. 8. GPR image illustrating the potential of the technique if beachrock is situated away from modern marine zone.

Fig. 9. Thin section images of beachrock deposits (North Africa, Mediterranean Sea). A - Moderately sorted oolitic grainstone with isopachous HMC rim (dull blue in CL) indicative for the lower intertidal zone. B - Well-sorted mixed bio-siliciclastic grainstone with syntaxial echinoderm overgrowth and circumgranular calcite, which is blue in CL with an outer band of violet colour. Isopachous fabric and faint Mn as CL activator indicate precipitation from oxidising water under shallow marine conditions in the lower intertidal zone.

Fig. 10. The coast at Torre Vieja (37°N, 00°E) and its beachrock deposit. The morphological setting suggest a Holocene age of the deposit while its OSL age (83±6 ka) suggests a RSL level similar to today during MIS 5a. For scale see person (ca 1.60 m).

Fig. 11. Illustration of indicative range of beachrock and associated error. The indicative range spans from upper shoreface to spray zone encompassing the range from mean low water level (MLW) to mean high water level (MHL). The midpoint of each zone is the reference water level. The minimum vertical error is half the tidal amplitude (*a/2*) and the maximum error is the tidal range (a_1+a_2). Tidal amplitude is half of the tidal range; a_1 = tidal amplitude between MTL and MLW; a_2 = tidal amplitude between MLT and MHW; *d* = maximum water depth of beachrock formation zone (typically upper shoreface); *s* = elevation of the spray zone.

Fig. 12. Location of beachrock deposits used for RSL reconstruction. See table 3 for references.

Fig. 13. Cross section at El Grine illustrating two Holocene beachrock deposits with their indicative meaning and associated uncertainty.

<u>Tables</u>

Table 1. Typical primary cement types and fabrics in beachrock. Listed are crystal form and orientation of c-axis on surface of components and in pore space in comparison to the water from which they precipitate, fabric of crystal assemblage, chemistry of precipitate and CL colours.

Table 2A. Description of beachrock samples dated using the OSL technique. The model used to determine the equivalent dose (D_e) is listed in Table 2C.

Table 2B. Analytical data used for OSL age estimation. For details on age modelling of carbonate-rich sediments see Nathan and Mauz (2008).

Table 2C. Analytical and statistical data used to estimate the equivalent dose (D_e). For details on statistics see Galbraith and Roberts (2012).

Table 3. Indicative meanings of beachrock with respect to the sea-level index point (SLIP) and limiting point. Reference water level for all SLIPS is the midpoint between the relevant water levels. Mean tide level (MTL) is the mean sea level (0 m); the vertical distance between mean high water (MHW) and mean low water (MLW) constitutes the tidal range which ideally oscillates symmetrically around the mean; tidal amplitude is half of the tidal range; a_1 = tidal amplitude between MTL and MLW; a_2 = tidal amplitude between MLT and MHW; *d* = maximum water depth of beachrock formation zone (typically upper shoreface); *s* = elevation of the spray zone.

Table 4. Beachrock characteristics and dating techniques used in studies. Listed are attributes used to establish the indicative meaning. Columns in italic indicate new interpretation inferred from our approach. Error of time is combined systematic and random uncertainty of respective dating technique (not listed). For details of indicative meaning and uncertainty see Table 2. Ar=aragonite; LMC=low magnesian calcite; HMC=high magnesian calcite.

Figure
Click here to download high resolution image

Figure 2

Figure 4
Click here to download high resolution image

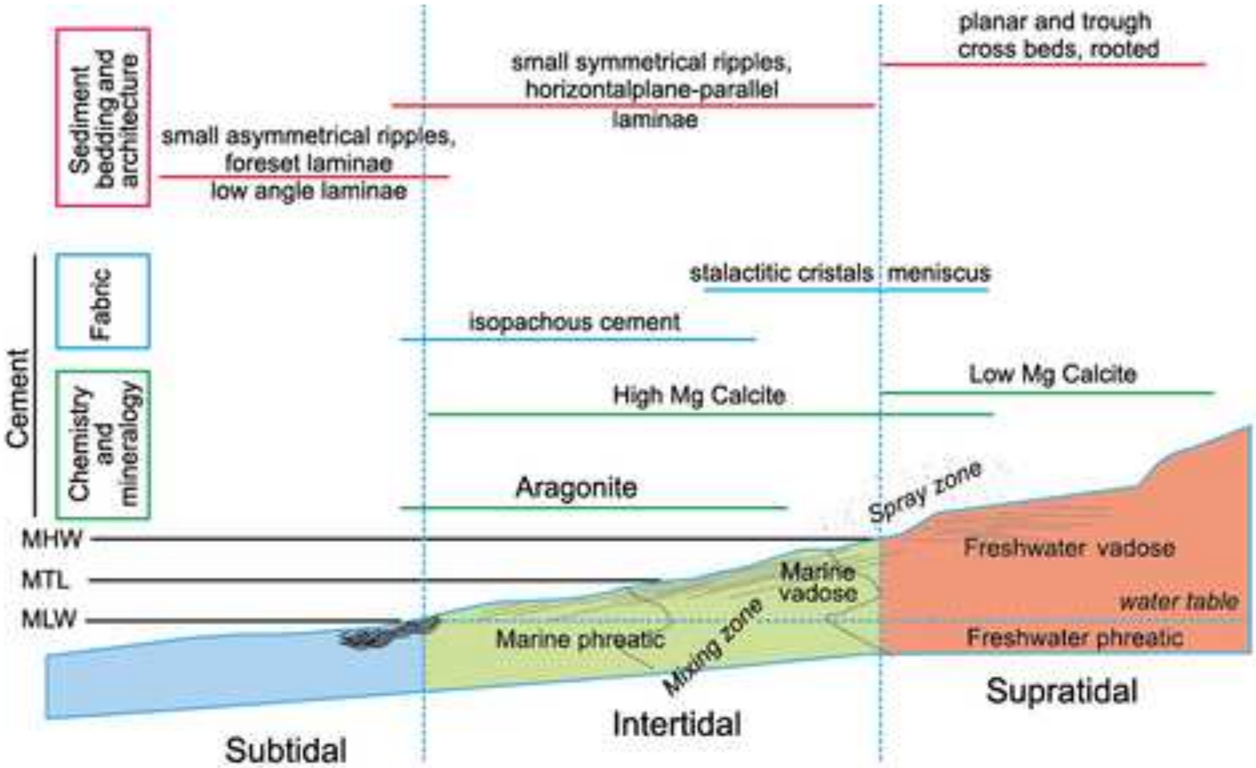

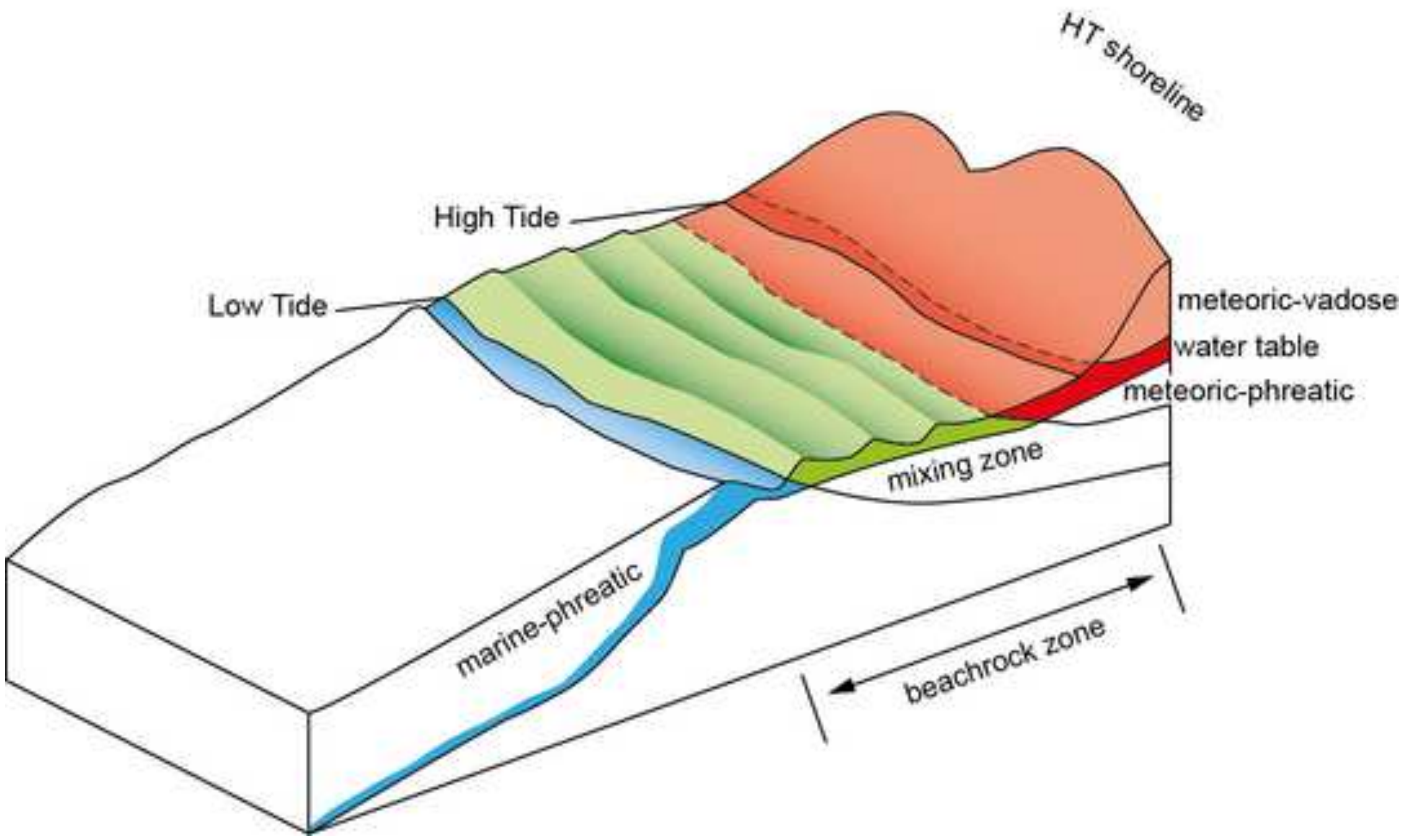

Figure 5

Click here to download high resolution image

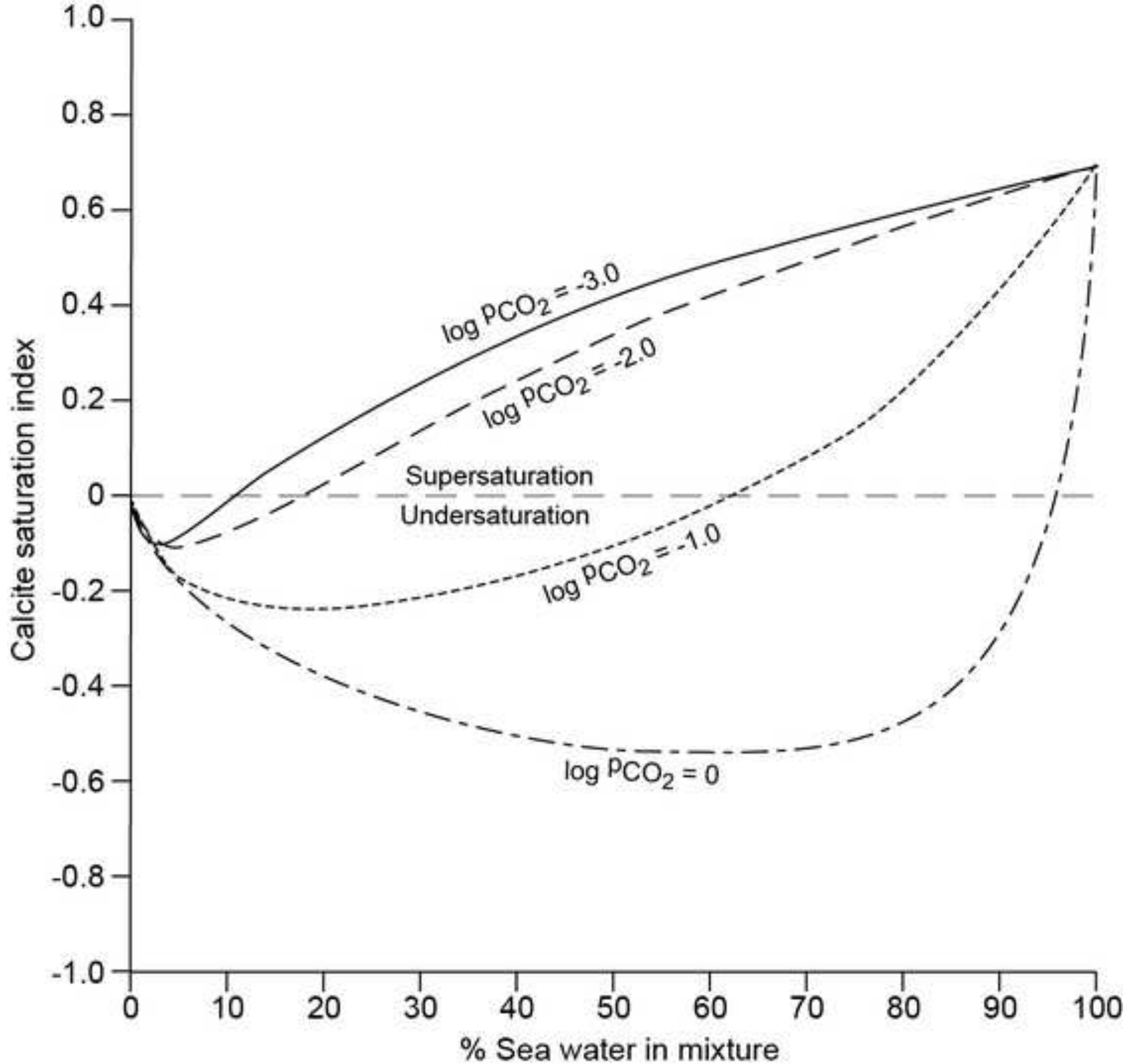

Figure 6
Click here to download high resolution image

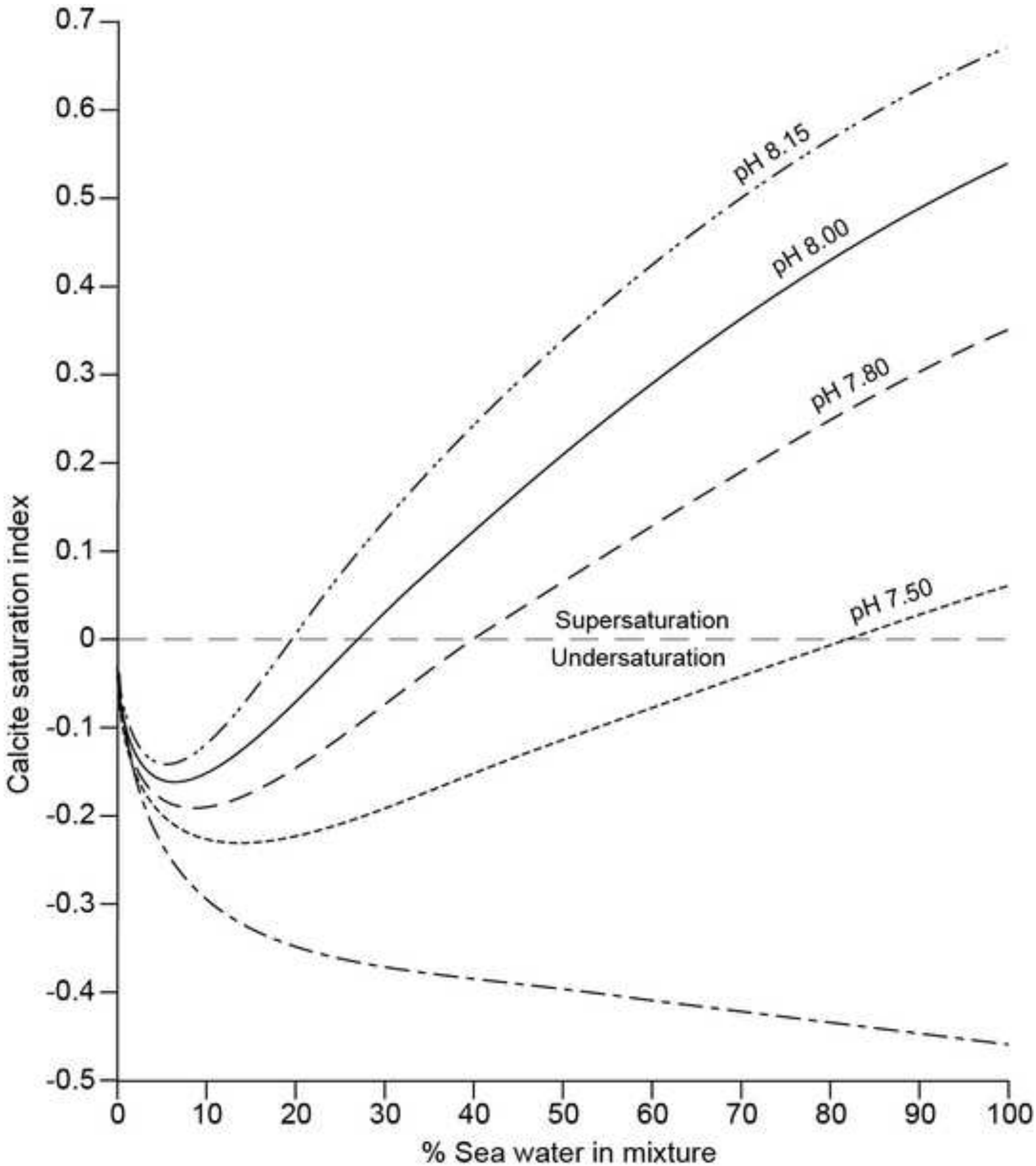

Figure 7
Click here to download high resolution image

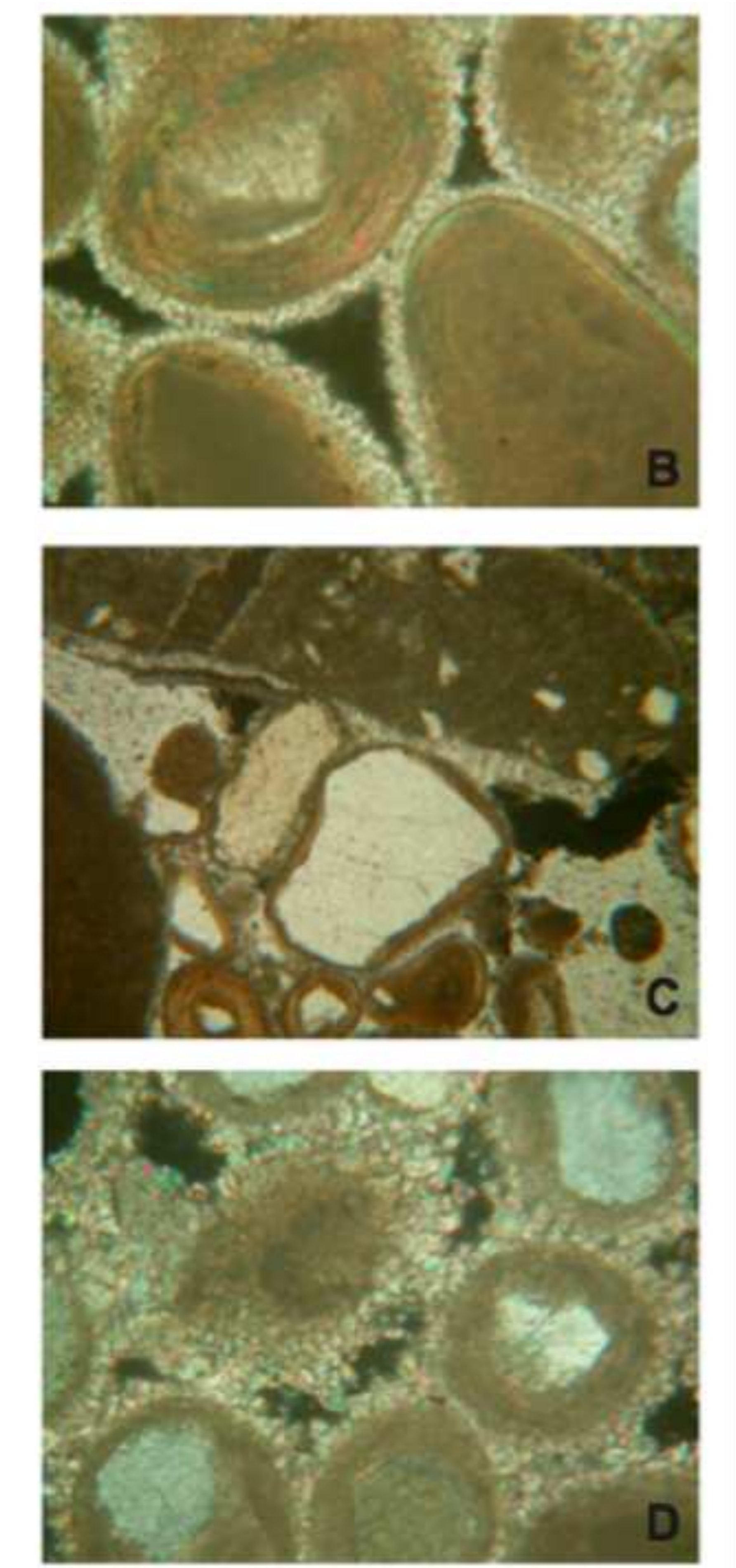

Figure 8
Click here to download high resolution image

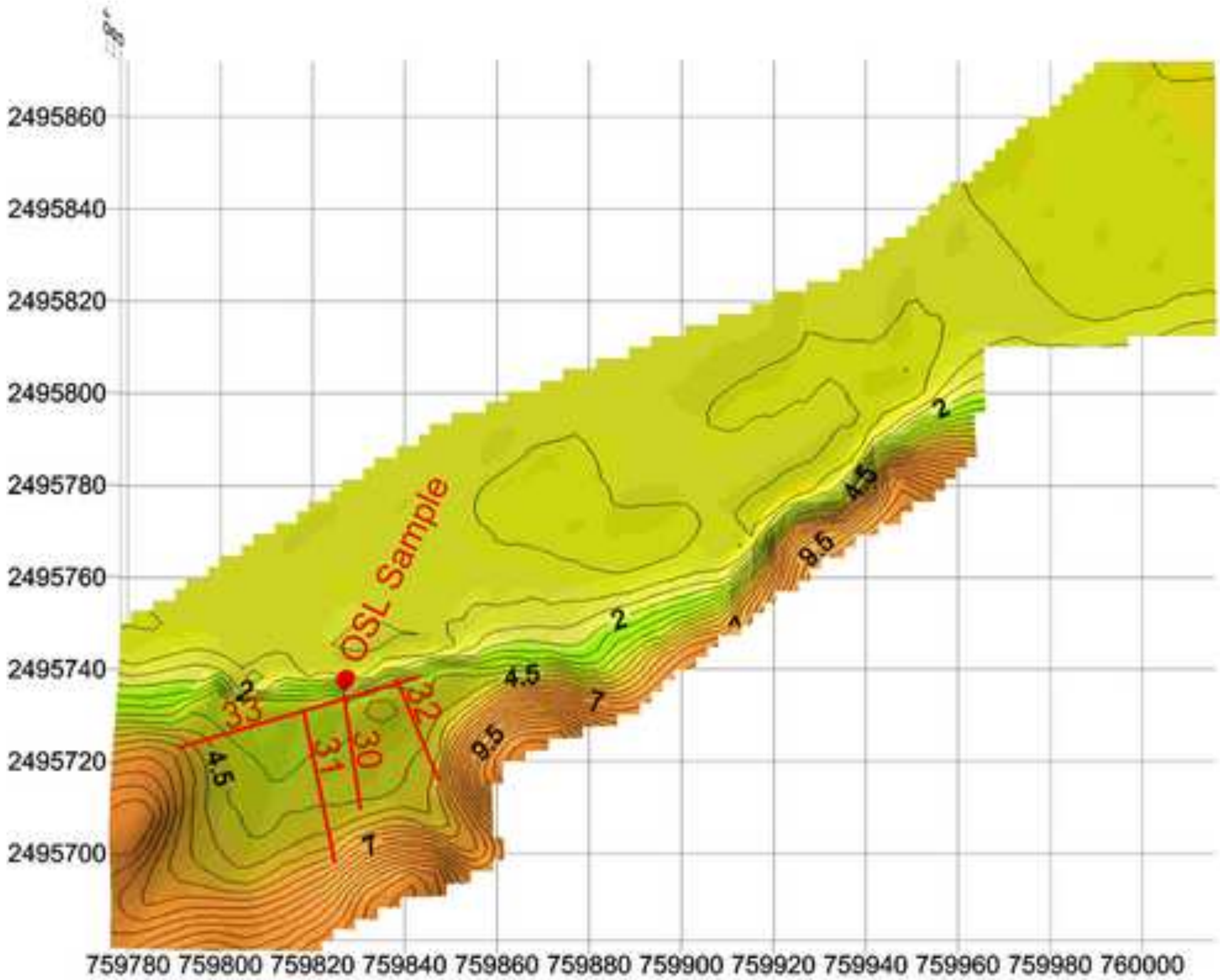

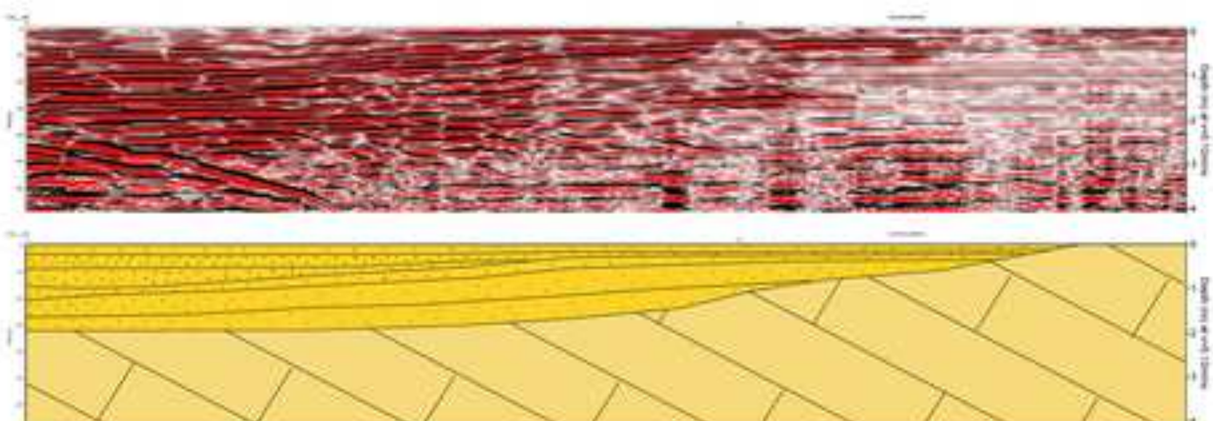

Figure 9A
Click here to download high resolution image

Figure 9B
Click here to download high resolution image

Figure 10
Click here to download high resolution image

Figure 11
Click here to download high resolution image

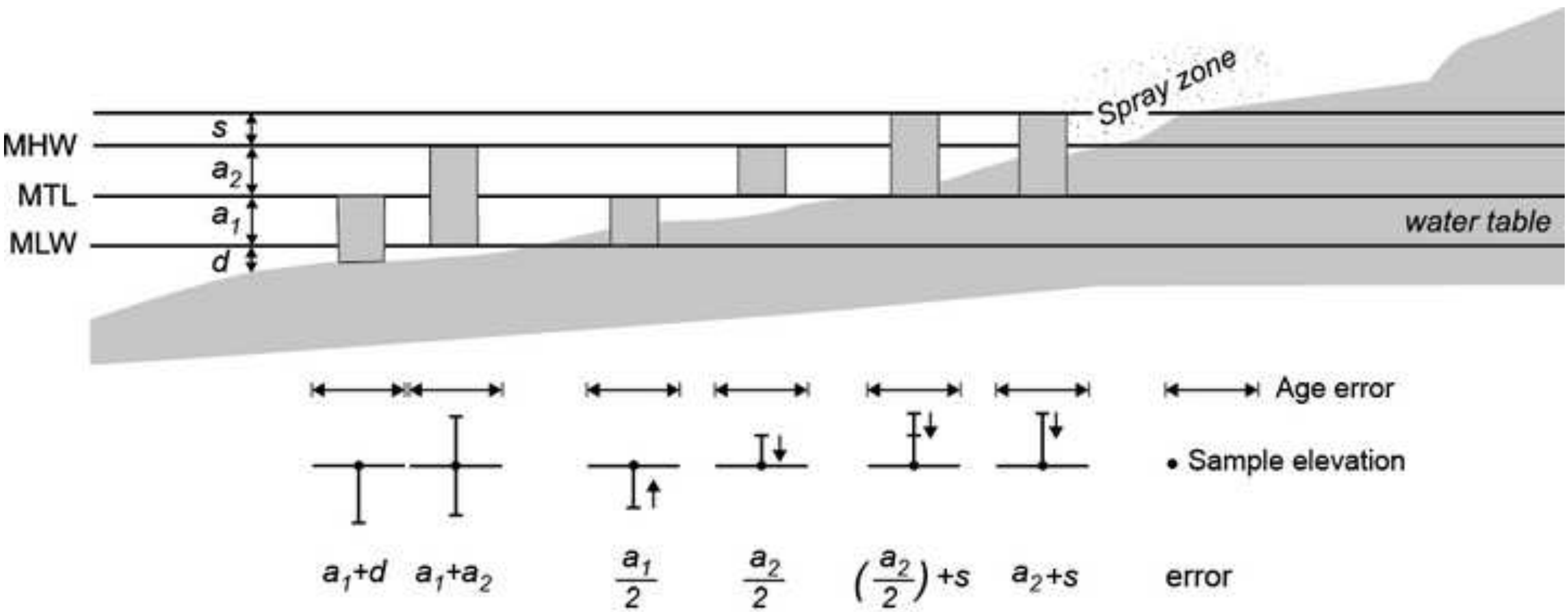

Figure 12
Click here to download high resolution image

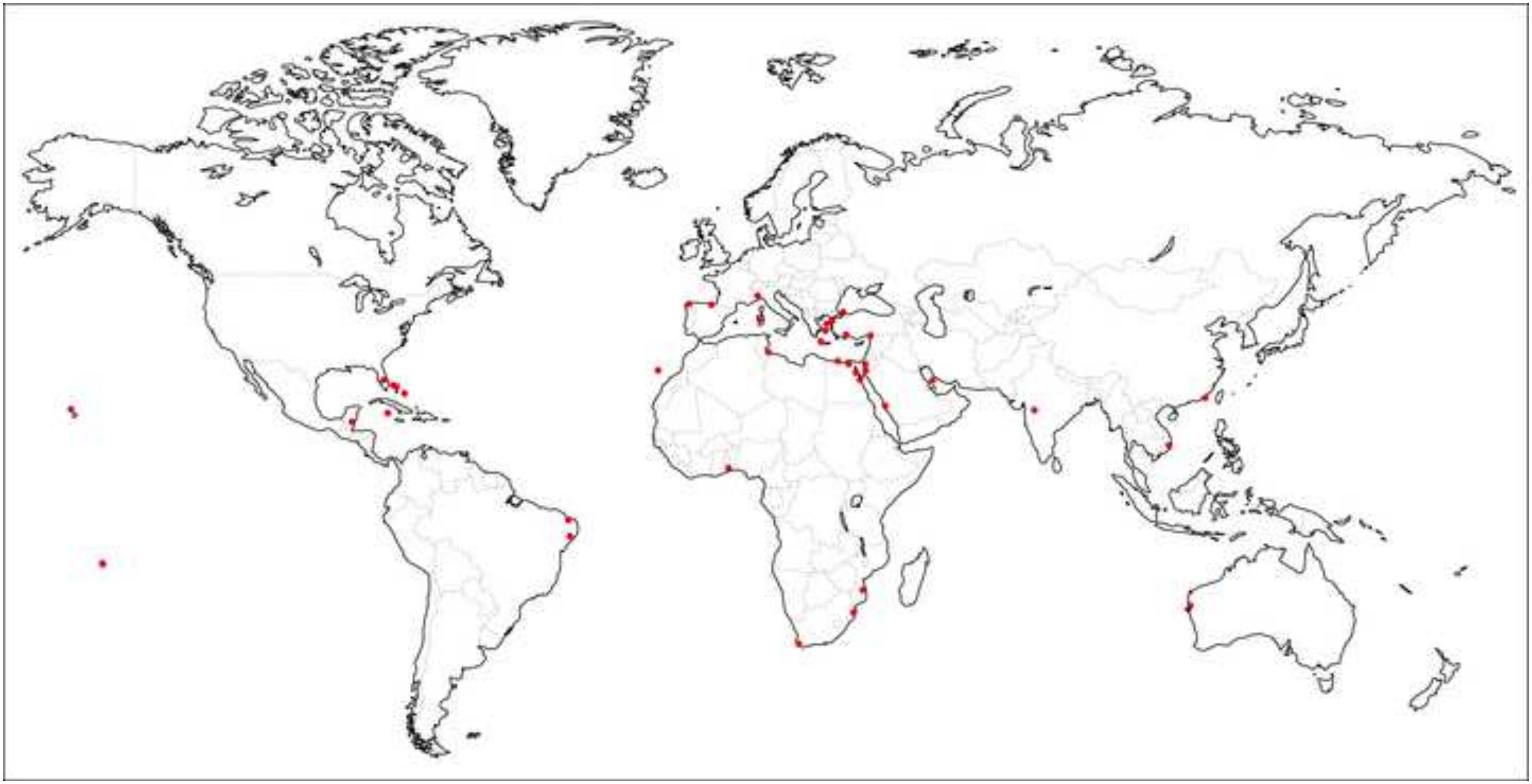

Figure 13
Click here to download high resolution image

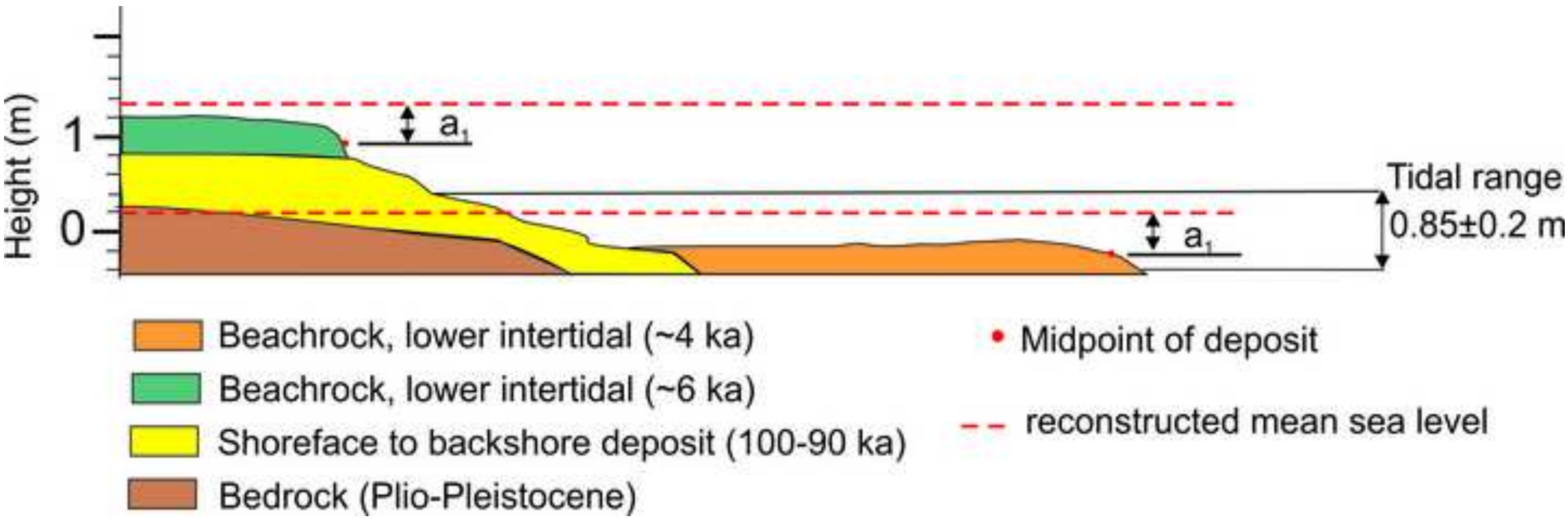

Table 1
Click here to download Table: Beachrock_table1.docx

Table 1.

Environment	Water	Grain Surfaces	Pore Space	Fabric	Chemistry/ Mineral	CL
Upper beach	Unmixed groundwater	Scalenohedral to rhombohedral (dog tooth), normal orientation	Equant subhedral, crystal size >30 μm; random orientation	Drusy to blocky, gravitational, syntaxial overgrowth	LMC or HMC	Blue
Lower beach to upper foreshore	Mixed water	Bladed, fibrous, normal orientation	Granular, crystal size 30 μm or empty	Gravitational, mosaic, syntaxial overgrowth	HMC	Subdued blue, violet
Lower foreshore to upper shoreface	Sea water	Microcrystalline, fibrous	Often empty, or granular	Symmetrical around grains	HMC, aragonite	orange
Lower shoreface	Sea water	Microcrystalline, fibrous	Empty, micrite (below fair-weather base)	Symmetrical around grains	HMC, aragonite	Bright orange

Table 2
Click here to download Table: beachrock_tables2.docx

Table 2A.

Sample code (LV)	Origin	Coordinates	D_e (median)±σ (Gy)	D_e (model, Gy)	OSL age (ka, ±1σ)
249	E-Mediterranean (Levant)	32.14N 34.49E	1.20±0.33	1.1±0.1	2.3±0.1
365	Levant	32.40N 34.56E	84±2	85±1	113±5
404	Levant	32.49N 34.57E	0.51±0.02	0.51±0.02	1.01±0.06
426	Iberia (Torre Vieja)	37.56N 00.42E	79±4	73±5	83±6
493	Gulf of Gabès	33.64N 10.55E	3.37±0.09	3.3±0.1	4.3±0.2
494	Gulf of Gabès	33.64N 10.56E	80±3	82±3	106±4
565	E-Arabia (Oman)	22.30N 59.56E	50±3	48±3	80±3

Table 2B.

Sample Code (LV)	Grain size (µm)	**Water content (%)**	**U (µg g^{-1})**	Th (µg g^{-1})	K (wt %)	$\dot{D}_{cosm}$ (Gy ka^{-1})	**Carbonate (%)**
249	180-250	8±3	0.399±0.018	0.626±0.063	0.169±0.010	0.212±0.010	71±4
365	150-200	5±3	1.353±0.036	0.763±0.058	0.227±0.010	0.153±0.008	60±3
404	200-250	5±3	0.247±0.012	0.288±0.069	0.194±0.010	0.21±0.01	65±4

426	200-250	5±2	1.156±0.032	1.785±0.069	0.474±0.014	0.21±0.01	75±4
493	200-300	5±2	1.440±0.035	0.765±0.039	0.072±0.006	0.21±0.01	87±5
494	90-150	6±2	1.732±0.045	0.679±0.058	0.201±0.010	0.098±0.004	69±4
565	200-300	5±2	1.708±0.045	0.796±0.085	0.122±0.009	0.172±0.009	90±3

Table 2C.

Sample code (LV)	**Aliquot# (accepted/ measured)**	**Aliquot size (mm)**	**Rejection**			**Descriptive Statistics**				**Statistical age model**
			D_0<53 Gy	**RR1/2**	**Dim/fit**	**σ (%)**	***c***	**s**	***k***	
249	33/72	3	n/a	18	21	43±5	-0.85	0.33	1.07	CAM
365	22/72	3	31	1	18	28±5	-1.06	-1.1	-0.25	CAM
404	42/96	5	n/a	35	19	24±3	0.86	0.25	2.79	median
426	22/24	3	-	-	2	39±6	-0.87	0.39	0.89	CAM
493	168/38	3	n/a	57	73	15±2	-0.37	0.16	0.38	CAM
494	31/96	3	22	18	25	17±3	0.94	0.189	1.61	CAM
565	23/111	3	57	24	7	24±4	-0.13	0.26	-0.07	CAM

Table 3
Click here to download Table: beachrock_Table3.docx

Table 3.

Sample Evidence	SLIP	Indicative Meaning	±
Irregularly distributed needles or isopachous fibres of aragonite or isopachous rims (bladed or fibrous) and micritic HMC cement and small-scaled trough cross stratification	Lower Intertidal	MTL to MLW	$a_1/2$
Irregularly distributed needles or isopachous fibres of aragonitic cement or isopachous rims (bladed or fibrous) and micritic HMC cement or HMC cement in stalactitic position and meniscus between grains and low angle seaward dipping tabular cross bedding with presence of keystone vugs	Upper intertidal	MHW to MTL	$a_2/2$
Irregularly distributed needles or isopachous fibres of aragonitic cement or isopachous rims (bladed or fibrous) and micritic HMC cement without bedding architecture information	Intertidal, undifferentiated	MHW to MLW	a_1+a_2
Small-scale trough cross stratification without cement fabric and chemistry information	Marine limiting	Below MTL	a_1+d
HMC cement in stalactitic position and meniscus between grains and internal sediments Low angle seaward dipping tabular cross bedding without keystone vugs and cement fabric and chemistry information Equant or subequant spar of LMC cement	Terrestrial limiting	Above MTL	a_2+s

Table 4

Click here to download Table: beachrock_table4.docx

Table 4.

Region	**Site**	**Refer-ence**	**Dating (material; technique)**	**Sediment bedding and architecture**	**Primary chemistry and mineralogy**	**Primary fabric**	**Other obser-vations**	**Markers used for indicative meaning**	**Authors' indicative meaning and uncertainty**	***New indicative meaning***	***Uncertainty***
South Africa	False bay (34° S)	Siesser, 1974	Bulk carbonate; ^{14}C	Not provided	LMC; Ar	Isopachous micritic rim	Extensive solution pits and vertical channels in the rock	Modern analogue; fossil assemblage; cement	Upper intertidal	*(MHW-MTL)/2*	*Tidal amplitude (MTL to MHW)*
Mozam-bique	Vilan-culo (22°S)	Siesser, 1974	Bulk carbonate; ^{14}C	Not provided	Ar	Isopachous fibrous needles	Intertidal fossil assem-blage	Modern analogue; fossil assemblage; cement	Intertidal	*(MHW-MLW)/2*	*Tidal range*
Brazil	Macau (1°S)	Bezerra et al., 2003	Articulated shell; ^{14}C	Trough-cross bedding	Not provided	Not provided	Not provided	Sediment bedding	Lower foreshore to upper shoreface, ±1 m	*MTL*	*undefined*
Brazil	Macau (1°S)	Bezerra et al., 2003	Articulated shell; ^{14}C	Seaward dipping swash-cross beds	Not provided	Not provided	Not provided	Sediment architecture	mid to lower foreshore, ±1 m	*MTL*	*undefined*
Greece	Mykonos (37°N)	Desruelles et al., 2009	Bulk carbonate; ^{14}C	Not provided	HMC	Isopachous small bladed rim	Not provided	Cement	Intertidal, ±0.5 m	*(MHW-MLW)/2*	*Tidal range*

Greece	Delos (37°N)	Desruelles et al., 2009	Bulk carbonate; ^{14}C	Not provided	HMC	Isopachous small bladed rim	Not provided	Cement	Intertidal, ±0.5 m	*(MHW-MLW)/2*	*Tidal range*
Greece	Delos (37°N)	Desruelles et al., 2009	Bulk carbonate; ^{14}C	Not provided	HMC	Internal sediments	Not provided	Cement	Intertidal, ±0.5 m	*(MHW-MLW)/2*	*Tidal range*
Greece	Rhenia (37°N)	Desruelles et al., 2009	Bulk carbonate; ^{14}C	Not provided	HMC	Isopachous small bladed rim	Not provided	Cement	Intertidal, ±0.5 m	*(MHW-MLW)/2*	*Tidal range*
Turkey	Kemer (36°N)	Desruelles et al., 2009	Cement; ^{14}C	Not provided	HMC	Internal sediments	Not provided	Cement	Intertidal, ±0.5 m	*(MHW-MLW)/2*	*Tidal range*
Turkey	Kemer (36°N)	Desruelles et al., 2009	Cement; ^{14}C	Not provided	Ar	Fibrous needles	Not provided	Cement	Intertidal, ±0.5 m	*(MHW-MLW)/2*	*Tidal range*
Turkey	Gozculer(36°N)	Desruelles et al., 2009	Cement; ^{14}C	Not provided	HMC	Isopachous fibrous rim	Not provided	Cement	Intertidal, ±0.5 m	*(MHW-MLW)/2*	*Tidal range*
Egypt	Alexandria (31° N)	El-Sayed, 1988	no dating	Not provided	HMC	Isopachous micritic rim	Not provided	Not provided	Not provided	*(MHW-MLW)/2*	*Tidal range*
Egypt	Safaga (34° N)	Holail and Rashed (1992)	no dating	Not provided	HMC, Ar	Isopachous micritic and fibrous rim	Not provided	Not provided	Not provided	*(MHW-MLW)/2*	*Tidal range*
Egypt	El Daba (31° N)	Holail and Rashed (1992)	no dating	Not provided	HMC, Ar	Isopachous micritic and fibrous rim	Not provided	Not provided	Not provided	*(MHW-MLW)/2*	*Tidal range*

Togo	Lomè (6° N)	Amieux et al., 1989	Mollusc shell; ^{14}C	Cross bedding	HMC, Ar, LMC	Isopachous micritic and fibrous rim	Not provided	Not provided	Not provided	*MLW to supratidal*	*Tidal range*
Belize	Cay (16°N)	Gischler and Lomando, 1997	Bulk carbonate; ^{14}C	Not provided	Ar; HMC	Isopachous micritic and fibrous rim	Not provided	Cement	Marine-phreatic zone	*(MTL+MLW)/2*	*Tidal amplitude (MHW to MTL)*
Vietnam	Cà Nà (10°N)	Michelli et al., 2008; Stattegger et al., 2013	Coral and Bivalve; ^{14}C	Cross bedding	HMC, Ar	Isopachous micritic and fibrous rim	Not provided	Sediment architecture; cement	Intertidal, ±1.15 m	*(MHW-MLW)/2*	*Tidal range*
Italy	Sardinia (40°N)	Lambeck et al., 2004	Bulk carbonate; ^{14}C	Cross bedding	HMC	Isopachous fibrous rim	Not provided	Cement	Palaeo-shoreline, +1 m, -5 m	*MTL*	*undefined*
Turkey	Thracia Black Sea (41°N)	Erginal et al., 2013	Bulk carbonate; ^{14}C	Not provided	LMC	Micritic	Not provided	Cement	Upper intertidal	*(MHW-MTL)/2*	*Tidal amplitude (MTL to MHW)*
Brazil	Cabelo (12°S)	Caldas et al., 2006	Bivalve; ^{14}C	Swash-cross-bedding	Not provided	Not provided	Not provided	Modern analogue; sediment architecture	Foreshore, ±1.4	*MTL*	*undefined*
Saudi Arabia	Al-Shoaiba (20°N)	Ghandour et al., 2014	no dating	Low-angle cross-bedding	Ar, HMC	Isopachous micritic and fibrous rim	Not provided	Cement	Marine-phreatic	*(MTL+MLW)/2*	*Tidal amplitude (MTL to MLW)*

Spain	Galicia (9°N)	Rey et al., 2004	no dating	Not provided	LMC	Isopachous fibrous rim	Meniscus	Not provided	supratidal	*MTL*	*undefined*
Spain	La Palma (28°N)	Calvet et al., 2003	Cement; ^{14}C	Not provided	Ar, HMC	Isopachous fibrous needle, isopachous spar rim, isopachous micritic rim	Meniscus	Cement	Intertidal to upper shoreface	*MTL*	*Tidal range*
USA	Florida (27°N)	Spurgeon et al., 2003	Bulk carbonate and cement; ^{14}C	Swash cross bedding and landward-dipping beds	LMC	Blocky spar rim; isopachous bladed spar rim	Not provided	Sediment architecture and cement	Supratidal	*MTL*	*undefined*
India	Maharastra (18°)	Badve et al., 1997	Gastropod; ^{14}C	Not provided	Ar	Isopachous fibrous rim	Fossil assem-blage	cement	Lower intertidal	(MTL+MLW)/2	*Tidal amplitude (MLW to MTL)*
Turkey	Parion (40°N)	Erginal, 2012	Bulk carbonate; ^{14}C	Not provided	HMC	Micritic	Meniscus, dissolution pits of meteoric water	Cement	Intertidal to supratidal	*MTL*	*undefined*
Israel	Tel Haratz (31°)	Bakler et al., 1985	Shell; ^{14}C	Low angle cross bedding	Ar, LMC	Isopachous fibrous needle rim, blocky	Not provided	Sediment architecture and cement	Intertidal to supratidal	(MHW-MTL)/2	*Tidal amplitude (MHW to MTL*

South Africa	Sodwana bay (27°S)	Ramsey; 1995; Ramsey and Cooper, 2002	U-series ($^{234}U/^{230}Th$)	Basal unit of a beachrock-aeolianite complex	Not provided	Isopachous fibrous rim, blocky equant	Not provided	Sediment architecture	Palaeo-sea level, ±1.5	*MTL*	*undefined*
Greece	Kalamaki, Crete (35°N)	Neumeier , 1998	Bulk carbonate and bioclasts; ^{14}C	Not provided	HMC	Micritic, Isopachous bladed spar rim		Cement	Intertidal	(MHW-MLW)/2	*Tidal range*
French Polynesia	Taraire (17°S)	Neumeier , 1998	Bulk carbonate; ^{14}C	Not provided	Ar	Isopachous fibrous needle rim		Cement	Intertidal	(MHW-MLW)/2	*Tidal range*
Egypt	Ras Garib (28° N)	Neumeier , 1998	Cement; ^{14}C	Not provided	Ar	Isopachous fibrous needle rim,	Not provided	Cement	Intertidal	(MHW-MLW)/2	*Tidal range*
Egypt	El Baida (25° N)	Neumeier , 1998	Cement; ^{14}C	Not provided	Ar	Isopachous fibrous needle rim,	Not provided	Cement	Intertidal	(MHW-MLW)/2	*Tidal range*
Saudi Arabia	Aqaba gulf (28°N)	Al-Ramadan, 2013	Bulk carbonate; ^{14}C	low angle seaward dipping cross beds	Ar; HMC	Isopachous fibrous needle, micritic	Not provided	Cement	Intertidal	(MHW-MLW)/2	*Tidal range*
Saudi Arabia	Arabic gulf (25° N)	Al-Ramadan, 2013	Bulk carbonate; ^{14}C	low angle seaward dipping cross	Ar; HMC	Isopachous fibrous needle,	Not provided	Cement	Intertidal zone	(MHW-MLW)/2	*Tidal range*

				beds		micritic					
Australia	Shark bay (25°S)	Neumeier, 1998	Bulk carbonate; ^{14}C	Not provided	Ar	Isopachous micritic, isopachous fibrous needle	Not provided	Cement	Intertidal	(MHW-MLW)/2	*Tidal range*
Greece	Lesvos (39°N)	Vacchi et al., 2012	Bioclasts; ^{14}C	Not provided	HMC	Isopachous Micritic, isopachous fibrous	Not provided	Cement	Palaeo-sea level, ±0.5	(MHW-MLW)/2	*Tidal range*
Tunisia	Bahiret el Biban (33°N)	Strasser et al., 1989	Bulk carbonate; ^{14}C	Seaward dipping beds	Ar; HMC	Isopachous fibrous needle; isopachous spar	Keystone vugs,	Sediment architecture and cement	Palaeo shoreline	(MHW-MLW)/2	*Tidal range*
Spain	Bilbao (43°N)	Arrieta et al., 2011	Modern fragments cemented in beachrock	Parallel laminated seaward dipping beds	Ar; HMC	Isopachous fibrous needle; micritic	Conglomeratic beds with imbricated clasts	Sediment architecture and cement	Shoreface to foreshore	(MTL+MLW)/2	*Tidal amplitude (MLW to MTL)*
China	Haishan Island (23°N)	Fuzhi and Youshen, 1988; Shen et al., 2013	Shell; ^{14}C	Low angle seaward dipping cross beds	Ar, LMC	Micritic, isopachous fibrous needle, spar	Fossil assemblage	Sediment architecture, fossils and cement	Semi-enclosed lagoon; Intertidal to supratidal	(MTL-MLW)/2	*Tidal amplitude (MHW to MTL)*
Bahamas	Bimini (25°N)	Strasser and Davaud, 1986	No dating	Seaward dipping tabular cross beds with keystone vugs	Ar	Isopachous fibrous needle	Keystone vugs	Sediment architecture and cement	Upper intertidal	(MTL-MLW)/2	*Tidal amplitude (MHW to MTL)*

Bahamas	Joulter Cays (25°N)	Strasser and Davaud, 1986	No dating	Seaward dipping tabular cross beds	Ar	Isopachous fibrous needle	Keystone vugs	Sediment architecture and cement	Upper intertidal	(MTL-MLW)/2	*Tidal amplitude (MHW to MTL)*
USA	Maui (21°N)	Meyers, 1987	No dating	Not provided	HMC	Isopachous rim	Meniscus	Cement	Marine vadose zone of the beach	(MTL-MLW)/2	*Tidal amplitude (MHW to MTL)*
Gran Cayman	Car (19°N)	Moore, 1973	No dating	Not provided	Ar, HMC	Isopachous fibrous, micritic or bladed rim	Not provided	Cement	Intertidal	(MHW-MLW)/2	*Tidal range*
Bahamas	San Salvador (24°N)	Kindler and Bain, 1993	Bulk carbonate; ^{14}C	Low angle seaward dipping planar lamination	Ar; LMC	Isopachous fibrous needle rim, micritic	Meniscus, keystone vugs	Stratification and cement	Intertidal to supratidal	*MTL*	*undefined*